Eur. Phys. J. C 5, 19–40 (1998)
DOI 10.1007/s100529800931

THE EUROPEAN PHYSICAL JOURNAL C

A search for neutral Higgs bosons in the MSSM and models with two scalar field doublets

OPAL Collaboration

K. Ackerstaff[8], G. Alexander[23], J. Allison[16], N. Altekamp[5], K.J. Anderson[9], S. Anderson[12], S. Arcelli[2], S. Asai[24], S.F. Ashby[1], D. Axen[29], G. Azuelos[18,a], A.H. Ball[17], E. Barberio[8], R.J. Barlow[16], R. Bartoldus[3], J.R. Batley[5], S. Baumann[3], J. Bechtluft[14], T. Behnke[8], K.W. Bell[20], G. Bella[23], S. Bentvelsen[8], S. Bethke[14], S. Betts[15], O. Biebel[14], A. Biguzzi[5], S.D. Bird[16], V. Blobel[27], I.J. Bloodworth[1], M. Bobinski[10], P. Bock[11], D. Bonacorsi[2], M. Boutemeur[34], S. Braibant[8], L. Brigliadori[2], R.M. Brown[20], H.J. Burckhart[8], C. Burgard[8], R. Bürgin[10], P. Capiluppi[2], R.K. Carnegie[6], A.A. Carter[13], J.R. Carter[5], C.Y. Chang[17], D.G. Charlton[1,b], D. Chrisman[4], P.E.L. Clarke[15], I. Cohen[23], J.E. Conboy[15], O.C. Cooke[8], C. Couyoumtzelis[13], R.L. Coxe[9], M. Cuffiani[2], S. Dado[22], C. Dallapiccola[17], G.M. Dallavalle[2], R. Davis[30], S. de Jong[12], L.A. del Pozo[4], A. de Roeck[8], K. Desch[8], B. Dienes[33,d], M.S. Dixit[7], M. Doucet[18], E. Duchovni[26], G. Duckeck[34], I.P. Duerdoth[16], D. Eatough[16], P.G. Estabrooks[6], E. Etzion[23], H.G. Evans[9], M. Evans[13], F. Fabbri[2], A. Fanfani[2], M. Fanti[2], A.A. Faust[30], L. Feld[8], F. Fiedler[27], M. Fierro[2], H.M. Fischer[3], I. Fleck[8], R. Folman[26], D.G. Fong[17], M. Foucher[17], A. Fürtjes[8], D.I. Futyan[16], P. Gagnon[7], J.W. Gary[4], J. Gascon[18], S.M. Gascon-Shotkin[17], N.I. Geddes[20], C. Geich-Gimbel[3], T. Geralis[20], G. Giacomelli[2], P. Giacomelli[4], R. Giacomelli[2], V. Gibson[5], W.R. Gibson[13], D.M. Gingrich[30,a], D. Glenzinski[9], J. Goldberg[22], M.J. Goodrick[5], W. Gorn[4], C. Grandi[2], E. Gross[26], J. Grunhaus[23], M. Gruwé[27], C. Hajdu[32], G.G. Hanson[12], M. Hansroul[8], M. Hapke[13], C.K. Hargrove[7], P.A. Hart[9], C. Hartmann[3], M. Hauschild[8], C.M. Hawkes[5], R. Hawkings[27], R.J. Hemingway[6], M. Herndon[17], G. Herten[10], R.D. Heuer[8], M.D. Hildreth[8], J.C. Hill[5], S.J. Hillier[1], P.R. Hobson[25], A. Hocker[9], R.J. Homer[1], A.K. Honma[28,a], D. Horváth[32,c], K.R. Hossain[30], R. Howard[29], P. Hüntemeyer[27], D.E. Hutchcroft[5], P. Igo-Kemenes[11], D.C. Imrie[25], K. Ishii[24], A. Jawahery[17], P.W. Jeffreys[20], H. Jeremie[18], M. Jimack[1], A. Joly[18], C.R. Jones[5], M. Jones[6], U. Jost[11], P. Jovanovic[1], T.R. Junk[8], J. Kanzaki[24], D. Karlen[6], V. Kartvelishvili[16], K. Kawagoe[24], T. Kawamoto[24], P.I. Kayal[30], R.K. Keeler[28], R.G. Kellogg[17], B.W. Kennedy[20], J. Kirk[29], A. Klier[26], S. Kluth[8], T. Kobayashi[24], M. Kobel[10], D.S. Koetke[6], T.P. Kokott[3], M. Kolrep[10], S. Komamiya[24], R.V. Kowalewski[28], T. Kress[11], P. Krieger[6], J. von Krogh[11], P. Kyberd[13], G.D. Lafferty[16], R. Lahmann[17], W.P. Lai[19], D. Lanske[14], J. Lauber[15], S.R. Lautenschlager[31], I. Lawson[28], J.G. Layter[4], D. Lazic[22], A.M. Lee[31], E. Lefebvre[18], D. Lellouch[26], J. Letts[12], L. Levinson[26], B. List[8], S.L. Lloyd[13], F.K. Loebinger[16], G.D. Long[28], M.J. Losty[7], J. Ludwig[10], D. Lui[12], A. Macchiolo[2], A. Macpherson[30], M. Mannelli[8], S. Marcellini[2], C. Markopoulos[13], C. Markus[3], A.J. Martin[13], J.P. Martin[18], G. Martinez[17], T. Mashimo[24], P. Mättig[26], W.J. McDonald[30], J. McKenna[29], E.A. Mckigney[15], T.J. McMahon[1], R.A. McPherson[28], F. Meijers[8], S. Menke[3], F.S. Merritt[9], H. Mes[7], J. Meyer[27], A. Michelini[2], S. Mihara[24], G. Mikenberg[26], D.J. Miller[15], A. Mincer[22,e], R. Mir[26], W. Mohr[10], A. Montanari[2], T. Mori[24], S. Mihara[24], K. Nagai[26], I. Nakamura[24], H.A. Neal[12], B. Nellen[3], R. Nisius[8], S.W. O'Neale[1], F.G. Oakham[7], F. Odorici[2], H.O. Ogren[12], A. Oh[27], N.J. Oldershaw[16], M.J. Oreglia[9], S. Orito[24], J. Pálinkás[33,d], G. Pásztor[32], J.R. Pater[16], G.N. Patrick[20], J. Patt[10], R. Perez-Ochoa[8], S. Petzold[27], P. Pfeifenschneider[14], J.E. Pilcher[9], J. Pinfold[30], D.E. Plane[8], P. Poffenberger[28], B. Poli[2], A. Posthaus[3], C. Rembser[8], S. Robertson[28], S.A. Robins[22], N. Rodning[30], J.M. Roney[28], A. Rooke[15], A.M. Rossi[2], P. Routenburg[30], Y. Rozen[22], K. Runge[10], O. Runolfsson[8], U. Ruppel[14], D.R. Rust[12], K. Sachs[10], T. Saeki[24], O. Sahr[34], W.M. Sang[25], E.K.G. Sarkisyan[23], C. Sbarra[29], A.D. Schaile[34], O. Schaile[34], F. Scharf[3], P. Scharff-Hansen[8], J. Schieck[11], P. Schleper[11], B. Schmitt[8], S. Schmitt[11], A. Schöning[8], M. Schröder[8], M. Schumacher[3], C. Schwick[8], W.G. Scott[20], T.G. Shears[8], B.C. Shen[4], C.H. Shepherd-Themistocleous[8], P. Sherwood[15], G.P. Siroli[2], A. Sittler[27], A. Skillman[15], A. Skuja[17], A.M. Smith[8], G.A. Snow[17], R. Sobie[28], S. Söldner-Rembold[10], R.W. Springer[30], M. Sproston[20], K. Stephens[16], J. Steuerer[27], B. Stockhausen[3], K. Stoll[10], D. Strom[19], R. Ströhmer[34], P. Szymanski[20], R. Tafirout[18], S.D. Talbot[1], P. Taras[18], S. Tarem[22], R. Teuscher[8], M. Thiergen[10], M.A. Thomson[8], E. von Törne[3], E. Torrence[8], S. Towers[6], I. Trigger[18], Z. Trócsányi[33], E. Tsur[23], A.S. Turcot[9], M.F. Turner-Watson[8], I. Ueda[24], P. Utzat[11], R. Van Kooten[12], P. Vannerem[10], M. Verzocchi[10], P. Vikas[18], E.H. Vokurka[16], H. Voss[3], F. Wäckerle[10], A. Wagner[27], C.P. Ward[5], D.R. Ward[5], P.M. Watkins[1], A.T. Watson[1], N.K. Watson[1], P.S. Wells[8], N. Wermes[3], J.S. White[28], G.W. Wilson[27], J.A. Wilson[1], T.R. Wyatt[16], S. Yamashita[24], G. Yekutieli[26], V. Zacek[18], D. Zer-Zion[8]

[1] School of Physics and Astronomy, University of Birmingham, Birmingham B15 2TT, UK
[2] Dipartimento di Fisica dell' Università di Bologna and INFN, I-40126 Bologna, Italy
[3] Physikalisches Institut, Universität Bonn, D-53115 Bonn, Germany
[4] Department of Physics, University of California, Riverside CA 92521, USA

[5] Cavendish Laboratory, Cambridge CB3 0HE, UK
[6] Ottawa-Carleton Institute for Physics, Department of Physics, Carleton University, Ottawa, Ontario K1S 5B6, Canada
[7] Centre for Research in Particle Physics, Carleton University, Ottawa, Ontario K1S 5B6, Canada
[8] CERN, European Organisation for Particle Physics, CH-1211 Geneva 23, Switzerland
[9] Enrico Fermi Institute and Department of Physics, University of Chicago, Chicago IL 60637, USA
[10] Fakultät für Physik, Albert Ludwigs Universität, D-79104 Freiburg, Germany
[11] Physikalisches Institut, Universität Heidelberg, D-69120 Heidelberg, Germany
[12] Indiana University, Department of Physics, Swain Hall West 117, Bloomington IN 47405, USA
[13] Queen Mary and Westfield College, University of London, London E1 4NS, UK
[14] Technische Hochschule Aachen, III Physikalisches Institut, Sommerfeldstrasse 26-28, D-52056 Aachen, Germany
[15] University College London, London WC1E 6BT, UK
[16] Department of Physics, Schuster Laboratory, The University, Manchester M13 9PL, UK
[17] Department of Physics, University of Maryland, College Park, MD 20742, USA
[18] Laboratoire de Physique Nucléaire, Université de Montréal, Montréal, Quebec H3C 3J7, Canada
[19] University of Oregon, Department of Physics, Eugene OR 97403, USA
[20] Rutherford Appleton Laboratory, Chilton, Didcot, Oxfordshire OX11 0QX, UK
[22] Department of Physics, Technion-Israel Institute of Technology, Haifa 32000, Israel
[23] Department of Physics and Astronomy, Tel Aviv University, Tel Aviv 69978, Israel
[24] International Centre for Elementary Particle Physics and Department of Physics, University of Tokyo, Tokyo 113, and Kobe University, Kobe 657, Japan
[25] Institute of Physical and Environmental Sciences, Brunel University, Uxbridge, Middlesex UB8 3PH, UK
[26] Particle Physics Department, Weizmann Institute of Science, Rehovot 76100, Israel
[27] Universität Hamburg/DESY, II Institut für Experimental Physik, Notkestrasse 85, D-22607 Hamburg, Germany
[28] University of Victoria, Department of Physics, P O Box 3055, Victoria BC V8W 3P6, Canada
[29] University of British Columbia, Department of Physics, Vancouver BC V6T 1Z1, Canada
[30] University of Alberta, Department of Physics, Edmonton AB T6G 2J1, Canada
[31] Duke University, Dept of Physics, Durham, NC 27708-0305, USA
[32] Research Institute for Particle and Nuclear Physics, H-1525 Budapest, P O Box 49, Hungary
[33] Institute of Nuclear Research, H-4001 Debrecen, P O Box 51, Hungary
[34] Ludwigs-Maximilians-Universität München, Sektion Physik, Am Coulombwall 1, D-85748 Garching, Germany

Received: 20 February 1998 / Published online: 13 July 1998

Abstract. A search is described for the neutral Higgs bosons h^0 and A^0 predicted by models with two scalar field doublets and, in particular, the Minimal Supersymmetric Standard Model (MSSM). The search in the Z^0h^0 and h^0A^0 production channels is based on data corresponding to an integrated luminosity of $25\,pb^{-1}$ from e^+e^- collisions at centre-of-mass energies between 130 and 172 GeV collected with the OPAL detector at LEP. The observation of a number of candidates consistent with Standard Model background expectations is used in combination with earlier results from data collected at the Z^0 resonance to set limits on m_h and m_A in general models with two scalar field doublets and in the MSSM. For example, in the MSSM, for $\tan\beta > 1$, minimal and maximal scalar top quark mixing and soft SUSY-breaking masses of 1 TeV, the 95% confidence level limits $m_h > 59.0\,GeV$ and $m_A > 59.5\,GeV$ are obtained. For the first time, the MSSM parameter space is explored in a detailed scan.

1 Introduction

The data accumulated with the OPAL detector at centre-of-mass energies of 130–172 GeV, corresponding to approximately 25 pb^{-1} of integrated luminosity, have opened up new kinematic domains for particle searches. We describe searches performed in these high energy data for neutral Higgs bosons which decay to hadrons or tau-leptons.

In the Standard Model (SM) [1], spontaneous symmetry-breaking is effected by the self-interaction of one scalar (Higgs) field doublet [2]. The model predicts one Higgs boson, $\mathrm{H}^0_{\mathrm{SM}}$, the mass of which is not specified. The OPAL search for $\mathrm{H}^0_{\mathrm{SM}}$ at $\sqrt{s} = 130$–$172\,\mathrm{GeV}$ has resulted in a lower bound on its mass of $m_{\mathrm{H}^0_{\mathrm{SM}}} > 69.4\,\mathrm{GeV}$ at the 95% confidence level (CL) [3].

Supersymmetry (SUSY) [4] is considered an attractive possible extension of the SM, since it provides a solution to one of the outstanding problems of the SM, that of the "hierarchy" of energy scales [5]. The implementation of SUSY requires at least two Higgs field doublets. There are exactly two in the Minimal Supersymmetric extension of the Standard Model (MSSM) [6]. These fields couple separately to up-type quarks for the first doublet, and to down-type quarks and charged leptons for the second dou-

[a] and at TRIUMF, Vancouver, Canada V6T 2A3
[b] and Royal Society University Research Fellow
[c] and Institute of Nuclear Research, Debrecen, Hungary
[d] and Department of Experimental Physics, Lajos Kossuth University, Debrecen, Hungary
[e] and Department of Physics, New York University, NY 1003, USA

blet, and have vacuum expectation values v_1 and v_2, respectively. Scalar field doublets that couple in this manner may exist more generally and the class of such models is known as Type II Two Higgs Doublet Model (2HDM) [7]. Here, 2HDM models will be understood to have no extra particles besides those of the SM and the two scalar doublets, and there is no mass relation between the different neutral and charged scalar field particles. In any two Higgs field doublet model, the Higgs sector comprises five physical Higgs bosons: two neutral CP-even scalars h^0 and H^0 (with masses satisfying $m_\mathrm{h} < m_\mathrm{H}$ by definition), one CP-odd scalar A^0 and two charged scalars $\mathrm{H}^\pm$. In this paper the searches are restricted to the neutral Higgs bosons h^0 and A^0. The heaviest neutral Higgs boson H^0 is likely to have a mass beyond the reach of LEP, and OPAL searches for $\mathrm{H}^\pm$ bosons have been published separately [8].

At the current $\mathrm{e^+e^-}$ centre-of-mass energies ($\sqrt{s}$) accessed by LEP, the h^0 and A^0 bosons are expected to be produced predominantly via two processes: the "Higgs-strahlung" process $\mathrm{e^+e^-}\to\mathrm{h^0Z^0}$ (where the Z^0 boson is on-shell) and the "pair production" process $\mathrm{e^+e^-}\to\mathrm{h^0A^0}$. Contributions from the $\mathrm{W^+W^-}$ and $\mathrm{Z^0Z^0}$ fusion processes account for a small part of the total production, except close to the kinematic limit of the $\mathrm{e^+e^-}\to\mathrm{h^0Z^0}$ process [9]. For these two principal processes, the cross-sections σ_hZ and σ_hA are related at tree-level to the SM cross-sections [10]:

$$\mathrm{e^+e^-}\to\mathrm{h^0Z^0} \;:\; \sigma_\mathrm{hZ} = \sin^2(\beta-\alpha)\;\sigma^\mathrm{SM}_\mathrm{HZ}, \qquad (1)$$

$$\mathrm{e^+e^-}\to\mathrm{h^0A^0} \;:\; \sigma_\mathrm{hA} = \cos^2(\beta-\alpha)\;\bar{\lambda}\;\sigma^\mathrm{SM}_{\nu\bar{\nu}}, \qquad (2)$$

where $\sigma^\mathrm{SM}_\mathrm{HZ}$ and $\sigma^\mathrm{SM}_{\nu\bar{\nu}}$ are the cross-sections for the SM processes $\mathrm{e^+e^-}\to\mathrm{H^0_{SM}Z^0}$ and $\mathrm{e^+e^-}\to\nu\bar{\nu}$, and $\bar{\lambda}$ is a kinematic factor, depending on m_h, m_A and $\sqrt{s}$, typically having values between 0.5 and 0.7 for the centre-of-mass energies under consideration. The angle β is defined in terms of the vacuum expectation values of the two scalar fields, $\tan\beta = v_2/v_1$, and α is the mixing angle of the CP-even $(\mathrm{h}^0,\mathrm{H}^0)$ fields. The coefficients $\sin^2(\beta-\alpha)$ and $\cos^2(\beta-\alpha)$ indicate complementarity in the cross-sections of the two processes, a feature which is exploited in deriving bounds for Higgs boson masses and other model parameters.

In the MSSM at tree level the following mass relations are predicted: $m_\mathrm{h} \le m_\mathrm{Z}$, $m_\mathrm{A} \le m_\mathrm{H}$, $m_\mathrm{Z} \le m_\mathrm{H}$ and $m_{\mathrm{H}^\pm} \ge m_{\mathrm{W}^\pm}$ [7]. Loop corrections, dominantly from the top and scalar top quarks ($\tilde{\mathrm{t}}$), strongly modify these mass relations and also have some moderate impact on the Higgs boson couplings [11]. The shift in ${m_\mathrm{h}}^2$, approximately proportional to $m_\mathrm{t}^4 \times \log({m_{\tilde{\mathrm{t}}}}^2/m_\mathrm{t}^2)$, can be several tens of GeV. While the top quark mass has been measured to be $m_\mathrm{t} = (175\pm5)\,\mathrm{GeV}$ [12], the mass of the scalar top quark $m_{\tilde{\mathrm{t}}}$ depends on the mixing in the $\tilde{\mathrm{t}}$ sector which, in turn, depends on several other parameters of the MSSM. However, even for a choice of SUSY parameters which maximises the mass shift, m_h should not exceed approximately 135 GeV [10]. Although this bound is beyond the ultimate reach of the LEP collider, a substantial fraction of this mass range is accessible.

In this work we undertake a more detailed examination of the MSSM parameter space than has been done in the past. The coefficients $\sin^2(\beta-\alpha)$ and $\cos^2(\beta-\alpha)$ which appear in (1) and (2) depend on a number of MSSM parameters which enter via mixing in the $\tilde{\mathrm{t}}$ sector and which will be summarised in a later section. We perform detailed scans over broad ranges of these parameters. Each of these scans is considered as an independent "model" within the MSSM, and results are provided for each. In increasing order of generality, they include: (A) Particular choices of parameters for "minimal" and "maximal" $\tilde{\mathrm{t}}$-mixing and soft SUSY-breaking masses fixed to be large as defined in [10] which are considered as the "benchmark case" and adopted by most search groups, (B) varying the parameters over a wide range, but keeping relations between some of them corresponding to minimal and maximal mixing, and (C) a "general" scan where the MSSM parameters are allowed to vary independently within wide, but reasonable, ranges.

The final-state topologies of the processes (1) and (2) are determined by the decays of the Z^0, h^0 and A^0 bosons. Since the Higgs bosons couple to fermions with a strength proportional to the fermion mass, the Higgs dominantly decays into pairs of the most massive fermions which are allowed by the kinematics, most notably b quarks and tau-leptons for the LEP mass range. For particular choices of the model parameters (e.g. for $\tan\beta < 1$) decays into $\mathrm{c\bar{c}}$ may be enhanced. For $2m_\mathrm{A} \le m_\mathrm{h}$, the process $\mathrm{h^0}\to\mathrm{A^0A^0}$ is also allowed and may even be the dominant decay, leading to more complex final states than those from direct decays into fermion pairs. In the MSSM, Higgs bosons may also decay into SUSY particles if allowed by kinematics. In particular, the decay into pairs of neutralinos ($\tilde{\chi}^0$) may lead to "invisible" Higgs decay channels[1] which must be considered in a full treatment of the model.

In searching for the process $\mathrm{e^+e^-}\to\mathrm{h^0Z^0}$, the fact is exploited that in most of the MSSM parameter space with $\tan\beta > 0.7$ the decay properties of the h^0 boson are essentially those of the SM Higgs boson. Thus, earlier OPAL searches for the $\mathrm{H^0_{SM}}$ boson [3], including those performed at energies above the Z^0 mass [13,14], are interpreted here as searches for $\mathrm{e^+e^-}\to\mathrm{h^0Z^0}$. The reduction of the search sensitivity due to $\sin^2(\beta-\alpha)$ in (1) is taken into account. Dedicated searches for "invisible" final states at $\sqrt{s} \approx m_\mathrm{Z}$ [15] are also included. Since these searches are published, we only summarise the results which are relevant for the present purpose. These searches for $\mathrm{H^0_{SM}}$ are also efficient for $\mathrm{e^+e^-}\to\mathrm{h^0Z^0}\to\mathrm{A^0A^0Z^0}$, sometimes after small modifications to the search.

In searching for the process $\mathrm{e^+e^-}\to\mathrm{h^0A^0}$, the following final states are most important: $(\mathrm{h^0}\to\mathrm{b\bar{b}})\,(\mathrm{A^0}\to\mathrm{b\bar{b}})$, $(\mathrm{h^0}\to\tau^+\tau^-)\,(\mathrm{A^0}\to\mathrm{q\bar{q}})$ and $(\mathrm{h^0}\to\mathrm{q\bar{q}})\,(\mathrm{A^0}\to\tau^+\tau^-)$. The searches in these channels using the data accumulated by OPAL between $\sqrt{s} = 130$ and 172 GeV have not been published. Therefore they are described in greater detail. The search for $\mathrm{h^0A^0}\to\mathrm{A^0A^0A^0}\to\mathrm{b\bar{b}b\bar{b}b\bar{b}}$ is important when

[1] In the MSSM R-parity is conserved and throughout this paper we assume that the lightest supersymmetric particle is the lightest neutralino, $\tilde{\chi}^0_1$

the decay $h^0 \to A^0 A^0$ is kinematically allowed and is also presented here for the first time for data taken above the Z^0 energy.

This paper starts in Sect. 2 with a short description of the OPAL detector, the data samples used and the various Monte Carlo simulations used to obtain the detection efficiencies and to estimate the backgrounds from SM processes. This is followed by a description of the event selections for the various $h^0 Z^0$ and $h^0 A^0$ channels in Sects. 3 and 4.

A new statistical method [16], summarised in Sect. 5, has been used to combine the results from different search channels and data sets taken at different centre-of-mass energies.

The model-independent and 2HDM results are summarised in Sect. 6, followed by those interpreted within the MSSM in Sect. 7.

Previous OPAL searches for the h^0 and A^0 bosons, based on data collected at $\sqrt{s} \approx m_Z$ are described in [13, 14]. The relevant publications from the other LEP collaborations describing neutral SUSY Higgs boson searches are listed in [17].

2 Experimental considerations

The present search includes data collected with the OPAL detector [18] in 1995 at $\sqrt{s} = 130$–$136\,\mathrm{GeV}$ ($5.2\,\mathrm{pb}^{-1}$), in 1996 at $\sqrt{s} = 161\,\mathrm{GeV}$ ($10.0\,\mathrm{pb}^{-1}$), and at 170–172 GeV ($10.4\ \mathrm{pb}^{-1}$). The results are combined with those from earlier searches [14] which are based on the analysis of up to 4.5 million hadronic Z^0 decays.

The OPAL detector is an apparatus with nearly complete solid angle coverage and excellent hermeticity. The central tracking detector consists of a high-resolution silicon microstrip vertex detector (μVTX) [19] with polar angle[2] coverage $|\cos\theta| < 0.9$, which immediately surrounds the beam-pipe, followed by a high-precision vertex drift chamber, a large-volume jet chamber, and z-chambers, all in a uniform 0.435 T axial magnetic field. A lead-glass electromagnetic calorimeter is located outside the magnet coil, which, in combination with the forward calorimeter, gamma catcher, and silicon-tungsten luminometer [20], complete the geometrical acceptance down to 33 mrad from the beam direction. The silicon-tungsten luminometer serves to measure the integrated luminosity using small-angle Bhabha scattering events [21]. The magnet return yoke is instrumented with streamer tubes for hadron calorimetry and is surrounded by several layers of muon chambers.

Events are reconstructed from charged-particle tracks and energy deposits ("clusters") in the electromagnetic and hadronic calorimeters. The tracks and clusters must pass a set of quality requirements similar to those used in previous OPAL Higgs boson searches [22]. In calculating the total visible energies and momenta, E_{vis} and $\mathbf{P}_{\mathrm{vis}}$, of events and of individual jets, corrections are applied against double-counting of energy in the case of tracks and associated clusters [23,24]. For the analysis presented here, charged particles and neutral clusters are grouped into jets using the Durham algorithm [25].

The tagging of jets originating from b quarks plays an important role in Higgs boson searches, since both h^0 and A^0 decay preferentially to $b\bar{b}$ over large domains of the two-field-doublet and MSSM parameter spaces. Primary and secondary vertices are reconstructed in three dimensions following two algorithms, using only tracks which pass an additional set of quality requirements. The first method (BTAG1) [26] considers all such tracks in a jet and attempts to fit them to a common vertex. Tracks are discarded from the vertex by an iterative procedure which drops the track with the largest χ^2 contribution to the vertex fit, until the largest χ^2 contribution is less than 4, with at least two tracks remaining. In the second method (BTAG2) [27], the intersection of all pairs of such tracks in a jet having impact parameter significance b/σ_b (where b is the impact parameter[3] and σ_b its error) greater than 2.5 are considered as seed vertices. The other tracks in the jet are added to the seed vertex in the order which results in the greatest vertex probability after each addition. The process continues until either all tracks in the jet are added or the resulting vertex probability falls below 1%, in which case the last track to have been added is dropped. If more than one acceptable vertex per jet is found via this algorithm, the best is chosen according to a set of criteria [26] involving track multiplicity and the vertex decay length significance $S \equiv L/\sigma_L$, where L is the vertex decay length[4] and σ_L its error. In both algorithms, S is then used to distinguish between b-flavoured hadron decays and background. The methods are found not to be fully correlated, and using them both adds discriminating power. Charged track impact parameters are also used to complement the secondary vertex algorithms via the forward multiplicity, defined as the number of tracks in a jet with $b/\sigma_b > 2.5$. Finally, semi-leptonic b-hadron decays are exploited by first identifying electrons via the method described in [28] and muons with the algorithm described in [29], and then considering the transverse momentum with respect to the corresponding jet axis.

The signal detection efficiencies and accepted background cross-sections are estimated using a variety of Monte Carlo samples. The HZHA generator [30] is used to simulate Higgs boson production processes. The detection

[2] OPAL uses a right-handed coordinate system where the $+z$ direction is along the electron beam and where $+x$ points to the centre of the LEP ring. The polar angle, θ, is defined with respect to the $+z$ direction and the azimuthal angle, ϕ, with respect to the horizontal, $+x$ direction

[3] The impact parameter is taken to be positive if in the two-dimensional projection the track path crosses the jet axis in the direction of the flight direction; otherwise it is negative

[4] The vertex decay length is the projection onto the jet direction of the distance between the primary vertex, as reconstructed for the event (see [26] for the algorithm), and the secondary vertex, as reconstructed for the jet. The decay length is taken to be positive if the vector that connects the primary to the secondary vertex is at an angle of less than 90° from the direction of the associated jet, and negative otherwise

Table 1. Summary of the searches for the SM Higgs boson at centre-of-mass energies of 161 and 170–172 GeV. For each channel the signal detection efficiencies for $m_{\mathrm{H^0_{SM}}} = 60$ and 70 GeV, the number of expected background events, and the number of events selected are given. The statistical error on the efficiencies is typically 1–4%

$\sqrt{s} = 161$ GeV				
Channel	$\epsilon(m_{\mathrm{H}}$=60 GeV)(%)	$\epsilon(m_{\mathrm{H}}$=70 GeV)(%)	Background	Data
Four-jet	30	31	0.75±0.08	0
Missing energy	56	41	0.90±0.10	1
Charged leptons $Z^0\to e^+e^-$	70	59	0.06±0.02	0
Charged leptons $Z^0\to\mu^+\mu^-$	75	73	0.04±0.03	0
Tau-lepton $Z^0\to\tau^+\tau^-$	24	17	0.10±0.03	0
Tau-lepton $Z^0\to q\bar{q}$	19	17	0.06±0.03	0
$\sqrt{s} = 170$–172 GeV				
Channel	$\epsilon(m_{\mathrm{H}}$=60 GeV)(%)	$\epsilon(m_{\mathrm{H}}$=70 GeV)(%)	Background	Data
Four-jet	27	28	0.88±0.07	1
Missing energy	47	41	0.55±0.05	0
Charged leptons $Z^0\to e^+e^-$	64	65	0.08±0.02	0
Charged leptons $Z^0\to\mu^+\mu^-$	69	71	0.06±0.03	0
Tau-lepton $Z^0\to\tau^+\tau^-$	27	22	0.41±0.03	0
Tau-lepton $Z^0\to q\bar{q}$	15	19	0.18±0.03	0

efficiencies are determined at fixed values of the Higgs boson masses using sample sizes varying between 500 and 10,000 events. Efficiencies at arbitrary masses are evaluated using spline fits in the $(m_{\mathrm{h}}, m_{\mathrm{A}})$ plane between these points. The background processes are simulated primarily by the following event generators: PYTHIA [31] ($(Z^0/\gamma)^*\to q\bar{q}(\gamma)$), EXCALIBUR [32] and grc4f [33] (four-fermion processes (4f)), BHWIDE [34] ($e^+e^-(\gamma)$), KORALZ [35] ($\mu^+\mu^-(\gamma)$ and $\tau^+\tau^-(\gamma)$), PHOJET [36] and Vermaseren [37] (hadronic and leptonic two-photon processes ($\gamma\gamma$)). The generated partons are hadronised using JETSET [31] and the resulting particles are processed through a full simulation [38] of the OPAL detector.

3 Searches for the process $e^+e^-\to h^0Z^0$

The OPAL searches for the SM process $e^+e^-\to H^0_{\mathrm{SM}}Z^0$ are interpreted as searches for the process $e^+e^-\to h^0Z^0$ via (1). The searches for H^0_{SM} using all data recorded at centre-of-mass energies up to 172 GeV are described in [3]. They make use of the following final states:

- "Four-jet": $(H^0_{\mathrm{SM}}\to b\bar{b})(Z^0\to q\bar{q})$ (q=u,d,s,c,b),
- "Missing energy": $(H^0_{\mathrm{SM}}\to q\bar{q})(Z^0\to\nu\bar{\nu})$ (q includes quarks and gluons),
- "Charged lepton": $(H^0_{\mathrm{SM}}\to q\bar{q})(Z^0\to e^+e^-, \mu^+\mu^-)$, and
- "Tau-lepton": $(H^0_{\mathrm{SM}}\to q\bar{q})(Z^0\to\tau^+\tau^-)$ and $(H^0_{\mathrm{SM}}\to\tau^+\tau^-)(Z^0\to q\bar{q})$.

The search in the missing energy channel is also sensitive to small contributions to H^0_{SM} production coming from the W^+W^- fusion process $e^+e^-\to\nu\bar{\nu}H^0_{\mathrm{SM}}$ while the search in the charged lepton channel is sensitive to those from the Z^0Z^0 fusion process $e^+e^-\to e^+e^-H^0_{\mathrm{SM}}$. These contributions are taken into account in the corresponding channels.

The results from these published searches at $\sqrt{s} =$ 161–172 GeV are summarised in Table 1, which lists the signal detection efficiencies for two Higgs boson masses in the range of interest, the residual expected number of background events and the number of selected candidate events in each search channel. As can be seen from the table, the selection criteria applied at $\sqrt{s} = 161$ GeV select one candidate in the missing energy channel, with a mass of (39.3±4.9) GeV, while those applied at 170–172 GeV select one candidate in the four-jet channel with a mass of (75.6±3.0) GeV. The earlier OPAL searches applied to Z^0 boson decays [14] selected one candidate in the charged lepton channel $\mu^+\mu^-H^0_{\mathrm{SM}}$ with a mass of (61.2±1.0) GeV (with 0.38±0.04 events expected from background) and two candidates in the missing energy channel with masses of (6.3±0.8) GeV and (24.8±3.0) GeV (with 2.3±0.4 events expected from background). All these candidates are considered as possible Higgs boson events when limits in the MSSM parameter space are computed.

The above searches are also sensitive to the process $e^+e^-\to h^0Z^0$ followed by $h^0\to A^0A^0$. The selection is slightly changed with respect to that described in [3] in the case of the four-jet and missing energy channels. In the four-jet channel the likelihood discriminant, as described later in Sect. 4.1, is reoptimised for the $Z^0A^0A^0$ final state. This increases the efficiency from 23% to 29%, while the back-

Table 2. Signal detection efficiencies for the searches for the SM Higgs boson, at centre-of-mass energies of 161 and 170–172 GeV, applied to the processes with $h^0 \to A^0A^0$ followed by $A^0 \to b\bar{b}$. The efficiencies are quoted for $m_h = 60$ GeV and $m_A = 30$ GeV, with typical statistical errors of $1-4\%$

$\sqrt{s} = 161$ GeV		
SM search	applied to the process	$\epsilon(\%)$
Four-jet	$(A^0A^0 \to b\bar{b}b\bar{b})(Z^0 \to q\bar{q})$	29
Missing energy	$(A^0A^0 \to q\bar{q}q\bar{q})(Z^0 \to \nu\bar{\nu})$	68
Charged leptons	$(A^0A^0 \to q\bar{q}q\bar{q})(Z^0 \to e^+e^-)$	60
Charged leptons	$(A^0A^0 \to q\bar{q}q\bar{q})(Z^0 \to \mu^+\mu^-)$	74
Tau-lepton	$(A^0A^0 \to q\bar{q}q\bar{q})(Z^0 \to \tau^+\tau^-)$	16
$\sqrt{s} = 170$–172 GeV		
SM search	applied to the process	$\epsilon(\%)$
Four-jet	$(A^0A^0 \to b\bar{b}b\bar{b})(Z^0 \to q\bar{q})$	34
Missing energy	$(A^0A^0 \to b\bar{b}b\bar{b})(Z^0 \to \nu\bar{\nu})$	59
Charged leptons	$(A^0A^0 \to q\bar{q}q\bar{q})(Z^0 \to e^+e^-)$	57
Charged leptons	$(A^0A^0 \to q\bar{q}q\bar{q})(Z^0 \to \mu^+\mu^-)$	73
Tau-lepton	$(A^0A^0 \to q\bar{q}q\bar{q})(Z^0 \to \tau^+\tau^-)$	17

ground expectation remains approximately equal. In the case of the missing energy channel at $\sqrt{s} = 161$ GeV a requirement on the jet resolution parameter, $y_{23} < 0.05$, limits the acceptance to two-jet events only. Removing this requirement, the detection efficiency for $h^0 \to A^0A^0$ ($m_h = 60$ GeV, $m_A = 30$ GeV) increases from 38% to 68% while the background increases from 0.9 to 1.1 events. For the decay of the A^0 boson, only the predominant $b\bar{b}$ final state is considered. For the charged lepton and tau-lepton channels, Monte Carlo simulations have demonstrated that the detection efficiencies for this two-stage process are close to those of the h^0 decay to fermion pairs. The detection efficiencies for the particular case of $m_h = 60$ GeV and $m_A = 30$ GeV, a point close to the boundary of the kinematically-allowed region for $h^0 \to A^0A^0$, are shown in Table 2. The candidate events selected are the same as for the corresponding SM channel analyses.

4 Searches for the process $e^+e^- \to h^0A^0$

In this section the searches for the MSSM process $e^+e^- \to h^0A^0$ for final states $(h^0 \to b\bar{b})(A^0 \to b\bar{b})$, $(h^0 \to \tau^+\tau^-)(A^0 \to q\bar{q})$, $(h^0 \to q\bar{q})(A^0 \to \tau^+\tau^-)$ and $(h^0 \to A^0A^0 \to b\bar{b}b\bar{b})(A^0 \to b\bar{b})$ are summarised. If the same branching ratios to $b\bar{b}$ and $\tau^+\tau^-$ are assumed for h^0 and A^0 as for H^0_{SM}, then the first three of the above final states account for approximately 90% of all h^0A^0 decays, in the portion of the (m_A, m_h) phase space where $m_A > m_h$. For points in this phase space where $m_h \geq m_A$ and the decay $h^0 \to A^0A^0$ is kinematically allowed, the last final state represents approximately 66% of decays of this type.

Table 3. Effect of the selection criteria on data, background (normalised to the integrated luminosity of the data) and signal simulation ($m_h = m_A = 55$ GeV) at the three centre-of-mass energies for the signal channel $h^0A^0 \to b\bar{b}b\bar{b}$. The quoted errors on the background are statistical

$\sqrt{s} = 130$–136 GeV					
Cut	Data	Total Bkg.	$q\bar{q}(\gamma)$	4f	$\epsilon(\%)$
(1)	1536	1489	1478	11	100
(2)	445	496	489	7	97
(3)	83	65.5	62.9	2.6	84
(4)	64	48.1	45.8	2.3	83
(5)	41	34.4	33.0	1.4	79
(6)	28	28.2	26.9	1.3	75
$\mathcal{L}$ cut	0	1.65±0.33	1.57	0.08	60
$\sqrt{s} = 161$ GeV					
Cut	Data	Total Bkg.	$q\bar{q}(\gamma)$	4f	$\epsilon(\%)$
(1)	1499	1399	1346	53	100
(2)	394	378	352	26	90
(3)	62	54.1	37.2	16.1	72
(4)	49	40.6	26.1	14.4	71
(5)	40	33.2	21.3	11.7	69
(6)	33	30.5	19.6	10.9	63
$\mathcal{L}$ cut	0	1.61±0.11	1.20	0.41	50
$\sqrt{s} = 170$–172 GeV					
Cut	Data	Total Bkg.	$q\bar{q}(\gamma)$	4f	$\epsilon(\%)$
(1)	1403	1254	1137	117	100
(2)	369	367	299	68	88
(3)	92	81.4	31.7	49.7	70
(4)	77	69.7	21.8	47.9	69
(5)	69	60.1	18.1	42.0	67
(6)	64	56.3	16.3	40.0	60
$\mathcal{L}$ cut	1	1.95±0.10	0.95	1.00	48

4.1 The channel $h^0A^0 \to b\bar{b}b\bar{b}$

The signature for events from the process $h^0A^0 \to b\bar{b}b\bar{b}$ is four energetic jets containing b-hadrons and a visible energy close to the centre-of-mass energy. As $\sqrt{s}$ changes from 130 GeV to 172 GeV, the background changes considerably in size and composition. At 130 GeV and 161 GeV the main background comes from $(Z^0/\gamma)^* \to q\bar{q}$ with or without initial state radiation accompanied by hard gluon emission. Four-fermion processes, in particular $e^+e^- \to W^+W^-$, play a minor role since the threshold for these processes is at most only marginally crossed. At 170–172 GeV this background becomes more important, while the $(Z^0/\gamma)^*$ background is reduced. Two-photon processes have a large cross-section at all energies; however, the se-

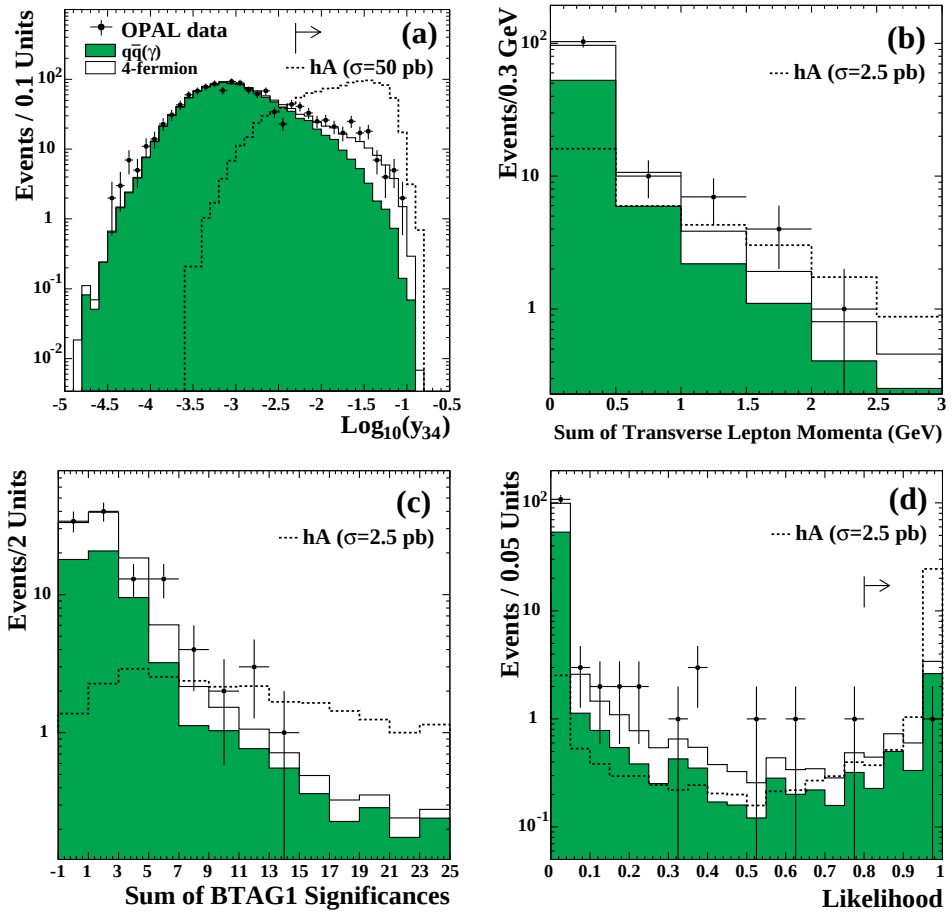

Fig. 1a–d. Selection variables relevant for the $h^0A^0 \to b\bar{b}b\bar{b}$ analysis. **a** The logarithm of the jet resolution parameter y_{34} after preselection requirements (1) and (2), **b** the sum of the two largest lepton transverse momenta after the preselection, **c** the sum of the two largest secondary vertex decay length significances of the BTAG1 algorithm (defined in Sect. 2) after the preselection, **d** the A^0h^0 likelihood distribution after the preselection. The three centre-of-mass energies are added for all histograms. The points represent the data. The shaded histograms show the $q\bar{q}$ background and the open histograms show the four-fermion background, normalised to the integrated luminosity of the data. Two-photon processes are not included. The dashed line histogram shows the expectation for A^0h^0 signal events with $m_A = m_h = 55\,\text{GeV}$, where the displayed production cross-sections have been chosen for visibility

lection requiring multihadronic final states with a visible energy close to $\sqrt{s}$ reduces them to a negligible level.

The selection proceeds in two phases. First, a preselection is applied to retain only those events which have some similarity to the signal. The events remaining after preselection are then analysed using a likelihood technique.

The preselection consists of the following requirements:

(1) The events must qualify as being hadronic final states as described in [39].
(2) The radiative process $e^+e^- \to (Z^0/\gamma)^* \to q\bar{q}\gamma$ is largely eliminated by requiring that the effective centre-of-mass energy, $\sqrt{s'}$, obtained by discarding the radiative photon from the event following [40], is greater than 110, 140 and 150 GeV for $\sqrt{s}$ = 130–136, 161, and 170–172 GeV, respectively.
(3) The events are reconstructed into four jets using the Durham algorithm [25]. The jet resolution parameter y_{34}, at which the number of jets changes from 3 to 4, is required to be larger than 0.005. The distribution of $\log y_{34}$ is shown in Fig. 1a.
(4) The value of the event shape C-parameter must be greater than 0.45. The C-parameter is defined as $C = 3(e_1e_2 + e_2e_3 + e_3e_1)$, with e_1, e_2 and e_3, being the eigenvalues of the normalised momentum tensor of the event [41]. It ranges from $C = 0$ for perfectly back-to-back two-jet events to $C = 1$ for perfectly spherical events.
(5) Each of the four reconstructed jets must contain at least two charged tracks and at least two electromagnetic calorimeter clusters.
(6) A fit of the jet four-momenta, in which the energy and momentum of the final state is constrained to that of the initial e^+e^- state, must yield a χ^2-probability larger than 0.01.

The results of the preselection are listed in Table 3. Except for the number of events retained after (1), the agreement between observed events and expected background predicted by the Monte Carlo simulation is good. The discrepancy after the first requirement can be explained by inaccurate modelling of events that radiatively return to the Z^0 and by not including the two-photon events in the Monte Carlo prediction. After a cut on $\sqrt{s'}$, these events are rejected and the background prediction from Monte Carlo describes the data well.

Next, a likelihood technique is used to classify the remaining events as either $(Z^0/\gamma)^* \to q\bar{q}(\gamma)$ (1), a four-fermion process (2), or $A^0h^0 \to b\bar{b}b\bar{b}$ (3). Three kinematic and six b-tagging variables are input to the likelihood. The kinematic quantities are: the smallest angle between any jet pair, the logarithm of the probability for a fit of the jet momenta with energy, momentum and equal di-jet mass constraint, and the smallest di-jet mass difference after the energy momentum conserving fit. For the b-tagging quantities used here, all vertices on which their calculation is

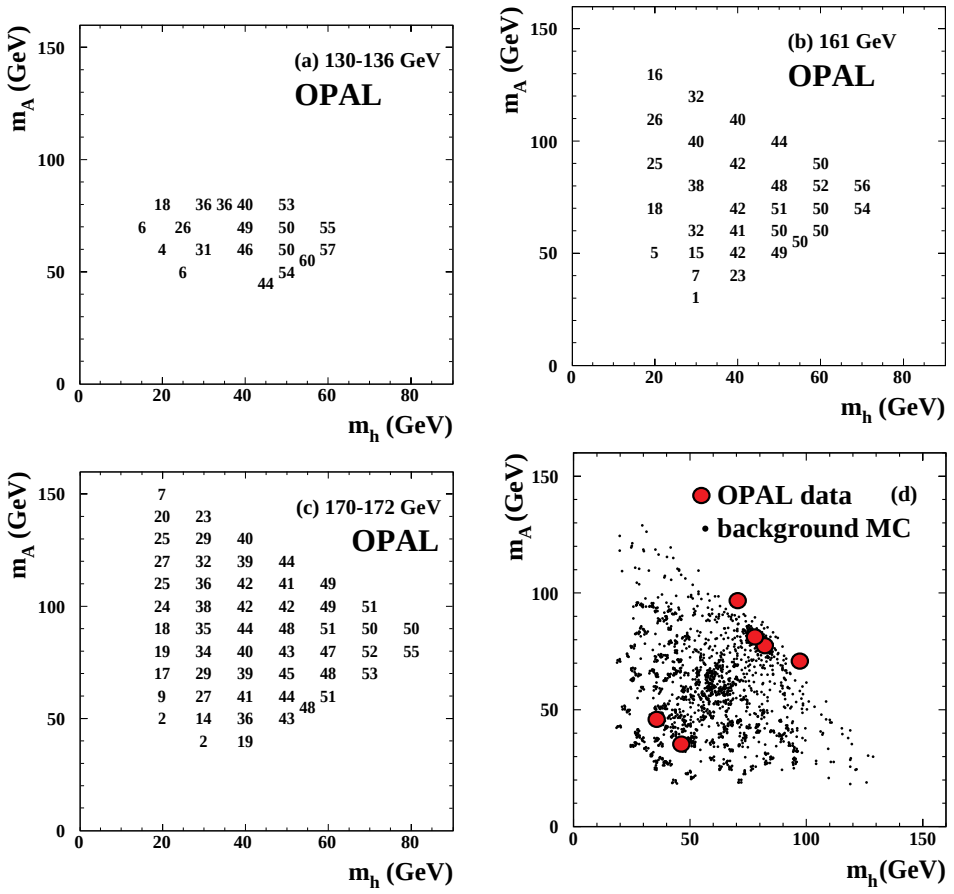

Fig. 2. a–**c** The efficiencies (in %) for the detection of $h^0A^0 \to b\bar{b}b\bar{b}$ at the three centre-of-mass energies in the $(m_h,\, m_A)$ plane. The numbers are shown only for $m_A \geq m_h$ due to the symmetry in m_h and m_A, **d** the position in the $(m_h,\, m_A)$ plane of the six possible mass combinations of the candidate event superimposed on the expected Standard Model background (scaled up by a factor of 100) for all centre-of-mass energies

based must contain at least two tracks, each having two hits in the $r-\phi$ and $r-z$ ladders of the μVTX detector. The calculation of forward multiplicities takes into account only tracks which have two hits in the $r-\phi$ and $r-z$ ladders of the μVTX detector. These quantities are (see Sect. 2 for a description): the sum of the two largest and the sum of the two smallest decay length significances in the four jets for vertices reconstructed with algorithm BTAG1, the sum of all decay length significances for vertices reconstructed with algorithm BTAG2, the sum of the two largest and the sum of the two smallest forward multiplicities, and the sum of the two largest transverse momenta with respect to the corresponding jet axis for identified leptons. For all of these quantities there is good agreement in their distributions between data and Monte Carlo background predictions, and as examples the distributions for the sum of the two largest lepton transverse momenta and the sum of the two largest decay length significances for the vertex algorithm BTAG1 are shown in Fig. 1b and c, respectively.

For each of these input variables (labelled by i) a normalised histogram $f_i^j(x_i)$ is constructed from the Monte Carlo for each of the two background classes and the signal (labelled by $j = 1, 2, 3$). For a single variable, the probability for an event to belong to class j is:

$$p_i^j(x_i) = \frac{f_i^j(x_i)}{\sum_{k=1}^{3} f_i^k(x_i)},$$

and the joint discriminating variable for class j is defined as:

$$\mathcal{P}^j(\mathbf{x}) = \frac{\prod_{i=1}^{9} p_i^j(x_i)}{\sum_{k=1}^{3}\prod_{i=1}^{9} p_i^k(x_i)},$$

where the product runs over the nine input variables. The signal likelihood is defined as:

$$\mathcal{L}^{\mathrm{Ah}}(\mathbf{x}) = \frac{\mathcal{P}^3(\mathbf{x})}{\sum_{j=1}^{3}\mathcal{P}^j(\mathbf{x})},$$

and is required to be greater than 0.8 for the final selection. The likelihood distribution is shown in Fig. 1d and over the entire range good agreement between the data and Monte Carlo background prediction can be observed. Some irreducible background from four-fermion processes also shows up as a small peak near a likelihood of 1. In total one event is selected, with a centre-of-mass energy of 172 GeV, while 1.65, 1.61 and 1.95 events are expected from the background simulations at $\sqrt{s}$ = 130–136, 161, and 170–172 GeV, respectively. The Poisson probability to select one or fewer events when 5.2 are expected is 2.3%.

The signal detection efficiencies are affected by the following main uncertainties, all expressed as relative percentages. The error from Monte Carlo statistics is typically $4-10\%$. However, near the region where the limit is set larger Monte Carlo samples were generated, and a fit is made through the grid of efficiencies in the $(m_h,\, m_A)$

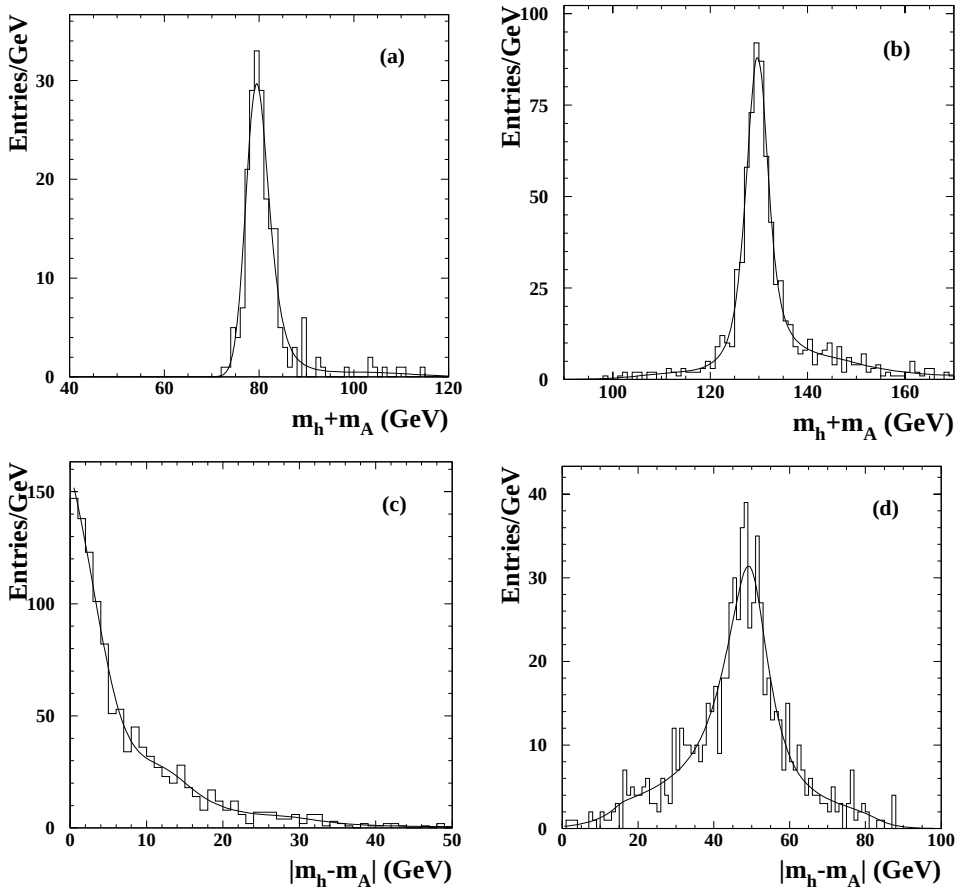

Fig. 3a–d. Mass resolution curves for $h^0A^0 \to b\bar{b}b\bar{b}$. **a** The mass sum of m_h and m_A for $m_h + m_A = 80\,\text{GeV}$, **b** the mass sum for $m_h + m_A = 130\,\text{GeV}$, **c** the mass difference of m_h and m_A for $m_h - m_A = 0$, **d** the mass difference for $|m_h - m_A| = 50\,\text{GeV}$. Only the combination with the smallest difference between measured and true mass sum or difference is plotted. The histograms show the simulated distributions and the solid lines represent smooth fitted functions

plane, so the efficiency at a certain mass point is effectively based on higher statistics. This results in a statistical error of approximately 1% in the region near the limit. The preselection requirements on $\sqrt{s'}$, y_{34}, and C were varied by amounts equivalent to the difference between the mean value of data and Monte Carlo. This results in an uncertainty estimate for the modelling of the preselection variables ranging from 3.5% to 7.6%, depending on the centre-of-mass energy. The uncertainty associated with the requirement on χ^2-probability was determined to be 2%. To assess the systematic uncertainty from the b-tagging, the impact parameter resolution was varied by 10%, and the b-hadron charged decay multiplicity was varied by 0.35 units [42]. The resulting errors range from 3.6% to 4.5% depending on the detector configuration (data taken in 1995 versus data taken in 1996.) The effect of binning in the likelihood was investigated by using a linear bin-to-bin interpolation. This gives rise to an uncertainty ranging from 0.0% to 0.4%. The theoretical uncertainty on the cross-section is estimated to be 1%. The systematic error on the integrated luminosity is 0.6% [21]. The total systematic uncertainty is calculated by adding the above uncertainties in quadrature. This gives uncertainties ranging from 5% to 9% depending on the centre-of-mass energy.

The residual background estimate has a statistical error of 20%, 7%, 5% at the 130–136, 161, 170–172 GeV centre-of-mass energies, respectively. The uncertainty from modelling the preselection was estimated in the same manner as for the efficiency, giving uncertainties ranging from 3.3% to 16%. The effects of impact parameter resolution and binning in the likelihood were also investigated in the same manner as for the efficiency. Uncertainties in the impact parameter resolution give errors between 15% and 23%. The effect of modelling the variables used in the likelihood selection is cross-checked by reweighting the Monte Carlo events in such a manner as to better approximate the data distributions within the ability of the Monte Carlo samples to represent the data. It should be noted that the agreement in these distributions before the reweighting procedure already gives a good χ^2 probability. This procedure yields errors ranging from 0.4% to 22%, and the corresponding error estimates on the signal detection efficiencies are negligible. In all cases errors due to the tracking resolution uncertainty were larger than those due to the reweighting procedure, and therefore the former are taken as the systematic errors for these two checks. The effect of binning on the likelihood for the background was estimated to range from 0.1% to 4.0%. The effect of modelling the Standard Model physics was investigated by comparing different Monte Carlo event generators. For the $Z^0/\gamma^* \to q\bar{q}$ background the results using the PYTHIA generator were compared to those using the HERWIG generator [43]. For the four-fermion background the EXCALIBUR and grc4f generators were compared. The uncertainties for the physics modelling range from 3.6% to 14%. The Monte Carlo generators have an uncer-

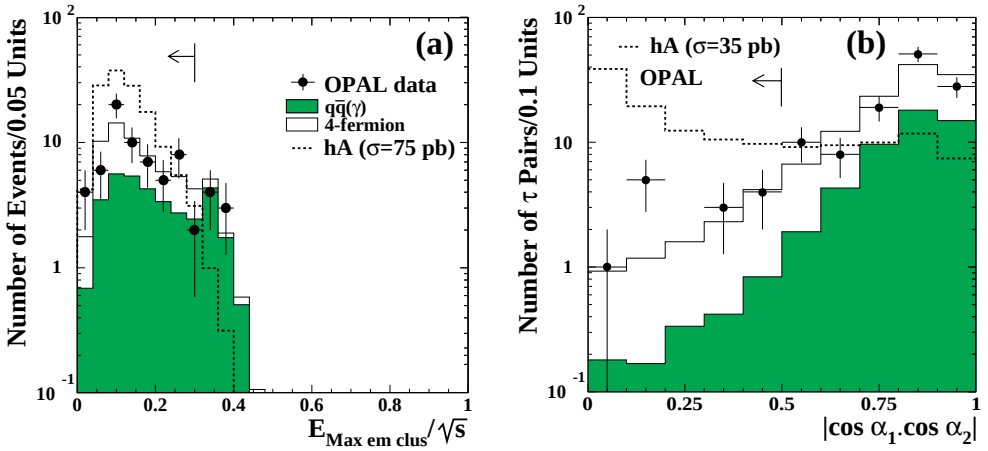

Fig. 4a,b. Selection variables relevant for the $h^0A^0 \to q\bar{q}\tau^+\tau^-$ analysis. **a** The energy of the most energetic electromagnetic cluster scaled by $\sqrt{s}$ after cut (3), **b** the pairwise isolation parameter (see text) after cut (4). The $\sqrt{s} = 161$ and 170–172 GeV data are added together. The points represent the data. The shaded histograms show the $q\bar{q}$ background and the open histograms show the four-fermion background, normalised to the integrated luminosity of the data. Two-photon processes are not included. The dashed histograms are simulated signals for $m_h = m_A = 55$ GeV, where the displayed production cross-sections have been chosen for visibility. The background simulations are normalised to the integrated luminosity of the data. Arrows indicate domains accepted by the selection

tainty on the calculated cross-sections of 0.5%. Including the error on the integrated luminosity of 0.6% [21], total relative uncertainties of 27%, 28%, 24% are assigned to the residual background estimates at centre-of-mass energies of 130–136, 161, 170–172 GeV, respectively.

To make use of the mass information in the calculation of exclusion limits, the hypothetical Higgs masses have to be determined. The four jets can be combined in three ways into two jet-pairs. The invariant masses of all jet-pair combinations of an event are considered. They are calculated using a kinematic fit assuming energy and momentum conservation (4C-fit). The mass distributions have a non-Gaussian shape. Since h^0 and A^0 cannot be distinguished, the mass difference $\Delta M = |m_A - m_h|$ and the sum $M = m_A + m_h$ are considered instead of the masses themselves. Figure 3 shows examples of these mass distributions at $\sqrt{s} = 172$ GeV. The resolution in M is roughly 3 GeV and does not vary with mass. The tails of the distribution of M, caused by the reconstructed jets not corresponding to the parton final states, exist largely above the mass peak for $M = 80$ GeV, whereas for $M = 130$ GeV they are present both above and below the nominal mass value. The shape of ΔM is independent of the mass sum. Its resolution is also approximately 3 GeV and the distribution shows substantial tails. Smooth functions fitted to these mass distribution histograms are used for exclusion limit calculations instead of the histograms themselves.

4.2 The channel $h^0A^0 \to \tau^+\tau^- q\bar{q}$

The $\tau^+\tau^- q\bar{q}$ final state can be produced via the processes $e^+e^- \to h^0A^0 \to \tau^+\tau^- q\bar{q}$ and $q\bar{q}\tau^+\tau^-$. These processes are characterised by a pair of tau-leptons and a pair of energetic hadronic jets. The backgrounds are predominantly from $(Z^0/\gamma)^* \to q\bar{q}(\gamma)$ and four-fermion processes. The search in these channels was restricted to the data recorded at the centre-of-mass energies $\sqrt{s} = 161$ and 170–172 GeV.

The selection begins with the identification of tau-leptons, identical to that in [3], using three algorithms which classify each tau-lepton candidates as decaying into an electron, a muon, or hadrons.

In the selection that follows, the tau-lepton direction is approximated by that of the visible decay products. If two tau-lepton candidates have momentum vectors separated by less than 23°, one being identified as a leptonic (electron or muon) decay and one as hadronic, the leptonic decay is chosen. The following selection, which is identical to that in [3] up to and including (4), was made:

(1) Events are required to have at least two tau-lepton candidates, each with electric charge $|q| = 1$, and at least nine charged tracks.
(2) Most of the two-photon and $e^+e^- \to (Z^0/\gamma)^*$ background events are eliminated by requiring that the energy in the forward detector, gamma catcher, and silicon-tungsten luminometer be less than 4, 10, and 10 GeV, respectively, that $|\cos\theta_{\rm miss}| < 0.97$ and that $P^T_{\rm vis} > 3$ GeV, where $\theta_{\rm miss}$ is the polar angle of the missing momentum vector and $P^T_{\rm vis}$ is the total transverse momentum of the event. In addition, the scalar sum of all track and cluster transverse momenta is required to be larger than 40 GeV. Accelerator-related backgrounds in the forward detectors which have not been fully simulated are taken into account via small corrections to the signal detection efficiencies.
(3) The remaining $(Z^0/\gamma)^* \to q\bar{q}(\gamma)$ background is partially suppressed by requiring that events contain at least four jets, reconstructed using the cone algorithm as in [3], where single electrons and muons from tau-lepton decays are allowed to be recognised as low-multiplicity "jets". Events with an energetic isolated

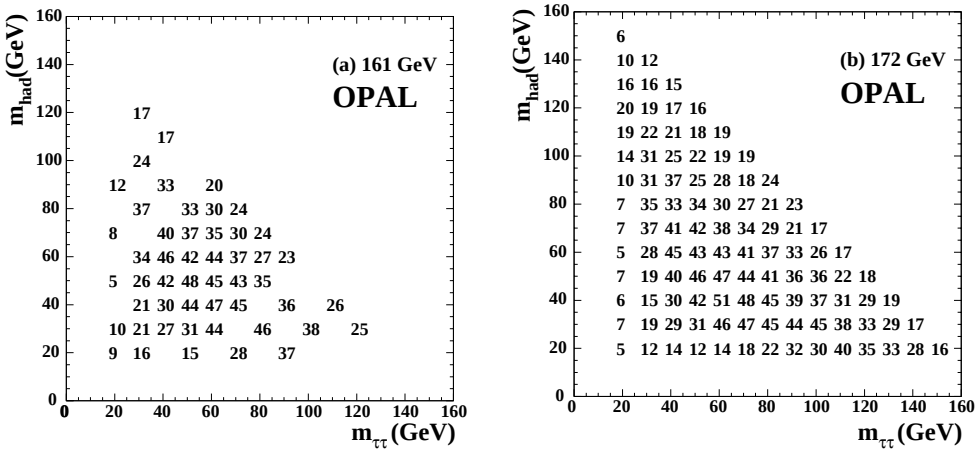

Fig. 5a,b. Efficiencies in percent for the signal process $h^0A^0 \to q\bar{q}\tau^+\tau^-$ in the $(m_{\tau\tau}, m_{had})$ plane at $\sqrt{s} = 161$ and 172 GeV, where $m_{\tau\tau}$ and m_{had} are the invariant masses of the tau-lepton pair and hadron jet-pair, respectively

photon are removed, where an energetic isolated photon is defined as an electromagnetic cluster with energy larger than 15 GeV and no track within a cone of 30° half-angle.

(4) To suppress the process $W^+W^- \to \ell\nu q\bar{q}'$, events are rejected if they contain any track or cluster with energy exceeding $0.3\sqrt{s}$. Figure 4a shows the distribution of the energy of the most energetic electromagnetic cluster scaled by $\sqrt{s}$, prior to this cut, for the data recorded at $\sqrt{s} = 161$–172 GeV, the expected backgrounds, and a simulated Higgs boson signal with $m_h = m_A = 55$ GeV.

(5) The three tau-lepton identification algorithms identify 2.3 τ candidates per signal event on average. Fake candidate pairs are removed by requiring that the sum of the track charges be zero and that the candidates satisfy a pairwise isolation requirement, $|\cos\alpha_i \cdot \cos\alpha_j| < 0.5$, where α_i is the angle between the direction of the i-th τ candidate and that of the nearest track not associated with it. The indices i, j run over all τ candidates with $i \neq j$. Figure 4b shows the distribution of this variable for pairs of tau-lepton candidates, for the data recorded at $\sqrt{s} = 161$–172 GeV, the expected backgrounds, and a simulated Higgs boson signal with $m_h = m_A = 55$ GeV. In those instances where more than one candidate pair passes the selection, the pair whose members have the lowest track multiplicity is chosen. If no distinction can be made, the candidate pair is chosen whose members have the highest value of the isolation parameter $R^{11/30}_{em+cd}$. Here $R^{11/30}_{em+cd}$ is the ratio of the sum of the electromagnetic cluster energies and charged track momenta within a cone of 11° half-angle centered on the τ candidate axis to that within a 30° half-angle cone.

The hadronic part of the event, obtained by excluding the tracks and clusters from the selected τ candidate pair, is then split into two jets using the Durham algorithm [25]. The invariant masses of the tau-lepton pair, $m_{\tau\tau}$, and of the hadron jet-pair, m_{had}, are calculated using only the tau-lepton and jet directions and requiring energy and momentum conservation. The resolutions of the mass distributions, later used in the calculation of exclusion limits (see Sect. 5), are determined from signal events by fitting a Gaussian distribution in an interval which excludes non-Gaussian tails, resulting in a typical error of 6 GeV on the reconstructed masses.

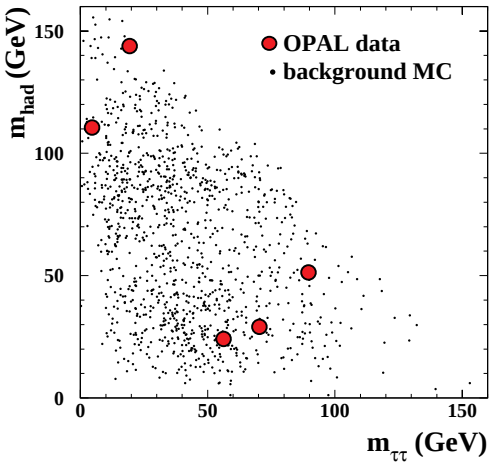

Fig. 6. The position in the $(m_{\tau\tau}, m_{had})$ plane of the $h^0A^0 \to \tau^+\tau^- q\bar{q}$ channel candidates, superimposed on that of the arbitrarily normalised expected Standard Model background, for $\sqrt{s} = 161$ and 170–172 GeV

The numbers of observed and expected events after each stage of the selection are given in Table 4 for $\sqrt{s} = 161$ GeV and 170–172 GeV. The agreement between the data and the expected background within the limited statistics demonstrates the adequate modelling of the selection criteria. The detection efficiency for a Higgs boson signal with $m_h = m_A = 55$ GeV is also given. Five events survive the selection while the background is estimated to be 1.29 events at $\sqrt{s} = 161$ GeV and 2.54 events at $\sqrt{s} = 170$–172 GeV. Figure 6 shows the positions of the surviving events in the $(m_{\tau\tau}, m_{had})$ plane superimposed on the expected background.

The detection efficiencies for various values of $m_{\tau\tau}$ and m_{had}, where $m_{\tau\tau}$ is the mass of the object (h^0 or A^0) decaying into the τ-pair and m_{had} is the mass of the object decaying into the jet-pair, are given in Fig. 5.

Table 4. Effect of the selection criteria on data, background (normalised to the integrated luminosity of the data) and signal simulation ($m_h = m_A = 55\,\text{GeV}$) at the two centre-of-mass energies for the signal channel $h^0A^0 \to \tau^+\tau^- q\bar{q}$. The quoted errors on the background are statistical

$\sqrt{s} = 161\,\text{GeV}$						
Cut	Data	Total Bkg.	$q\bar{q}$	4f	$\gamma\gamma$	$\epsilon(\%)$
(1)	402	398.0	92.8	18.3	286.9	67
(2)	45	44.7	30.9	13.3	0.5	62
(3)	32	30.1	19.6	10.1	0.4	61
(4)	26	22.7	14.3	8.0	0.4	57
(5)	0	1.29±0.24	0.41	0.88	<0.21	46
$\sqrt{s} = 170$–$172\,\text{GeV}$						
Cut	Data	Total Bkg.	$q\bar{q}$	4f	$\gamma\gamma$	$\epsilon(\%)$
(1)	358	306.9	75.2	36.8	194.9	67
(2)	50	55.1	23.6	31.2	0.3	63
(3)	37	40.1	15.2	24.7	0.2	61
(4)	31	32.3	11.0	21.3	<0.22	57
(5)	5	2.54±0.24	0.21	2.33	<0.22	46

The efficiencies are affected by the following uncertainties: Monte Carlo statistics, typically 2.2%; uncertainty in the tau-lepton identification efficiency, 3.6%; uncertainties due to modelling of selection variables excluding the tau-lepton identification, 6.3%; uncertainties in the modelling of fragmentation and hadronisation, 2.4%; and uncertainty on the integrated luminosity, 0.6% [21]. Taking these uncertainties as independent and adding them in quadrature results in a total systematic uncertainty of 7.9% (relative errors). The uncertainties due to the modelling of selection variables, including those used in tau-lepton identification, were estimated by displacing the cut values by an amount corresponding to the difference between the means of the data and background Monte Carlo distributions. Using the same techniques, the uncertainty in the number of expected background events was estimated to be 32%, dominated by the systematic uncertainty associated with the requirement on $|\cos\alpha_i \cdot \cos\alpha_j|$, which is steeply falling for background at the position of the cut. Because of this predominance of one single selection variable in the uncertainty on the number of expected background events, the background is not subtracted when computing limits.

4.3 The channel $h^0A^0 \to b\bar{b}b\bar{b}b\bar{b}$

When $2m_A \leq m_h$ the decay $h^0 \to A^0A^0$ is allowed and may be dominant. In these cases the process $e^+e^- \to h^0A^0 \to A^0A^0A^0$ can have a large branching ratio for the final state $b\bar{b}b\bar{b}b\bar{b}$. Due to the presence of six b quarks in the expected signature, the events are characterised by a large number of jets and a large charged track multiplicity. To reduce backgrounds b-tagging plays a crucial role. The main background is from $(Z^0/\gamma)^* \to b\bar{b}g(\gamma)$ with hard gluon emission. At 161 and 170–172 GeV four-fermion processes also result in a small contribution. Backgrounds from two-photon processes are reduced to a negligible level by the event selection.

The initial event selection follows that for $h^0A^0 \to b\bar{b}b\bar{b}$ described in Sect. 4.1. The data samples from $\sqrt{s} = 130$–172 GeV are all used. The following requirements are made:

(1) The events must qualify as hadronic final states as described in [39].
(2) Jets are reconstructed using the Durham [25] algorithm with $y_{\text{cut}} = 0.0015$. Events having five or more jets are retained.
(3) As in the $h^0A^0 \to b\bar{b}b\bar{b}$ analysis, the radiative process $e^+e^- \to (Z^0/\gamma)^* \to q\bar{q}\gamma$ is largely eliminated by a requirement on the effective centre-of-mass energy, in this case $\sqrt{s'} > 110\,\text{GeV}$. The distribution of the number of jets for events with four or more jets after application of this requirement is shown in Fig. 7a for data and simulated background and signal.
(4) The number of charged tracks for the signal process is quite large, but the backgrounds from $(Z^0/\gamma)^* \to q\bar{q}(\gamma)$ and four-fermion processes have long tails extending to high multiplicities (see Fig. 7b). Candidate events are required to have more than 35 charged tracks.
(5) Three or more jets are required to show evidence for b quark flavour, using the b-tagging algorithms discussed in Sect. 2 (BTAG1 [26] and BTAG2 [27]). The secondary vertices used in these methods are in addition required to have at least two tracks each with two μVTX r-ϕ hits assigned [3]. The decay length significances S, ordered in decreasing significance, must be successively $S > 8$, 4, 3 for BTAG1 vertices and $S > 8$, 5, 3 for BTAG2 vertices. Events must pass either the BTAG1 requirements or the BTAG2 requirements. The distributions of the significance of the most significant and the third most significant vertex for the BTAG1 algorithm are shown in Fig. 7c and d for events passing requirement (3).

Distributions of the variables relevant for the selection are shown in Fig. 7a–d for the 130–136 GeV, 161 GeV and 170–172 GeV data combined. Within the limited statistics, the agreement of the data with the Monte Carlo simulations is reasonable, except that it was found that the PYTHIA simulation of $e^+e^- \to (Z^0/\gamma)^* \to q\bar{q}\gamma$ underestimates the number of events with five or more jets. This discrepancy arises only in the Z^0 radiative return peak. The loose requirement on $\sqrt{s'}$ was made to decrease the number of Z^0 radiative return events in order to reduce the effect of this uncertainty on the final selection, while maintaining a high signal efficiency. This discrepancy, which would be eliminated with a harder requirement on $\sqrt{s'}$, vanishes subsequently with the application of the remainder of the selection.

The numbers of events passing each requirement, compared with estimates from the background simulations normalised to the integrated luminosities, are shown in

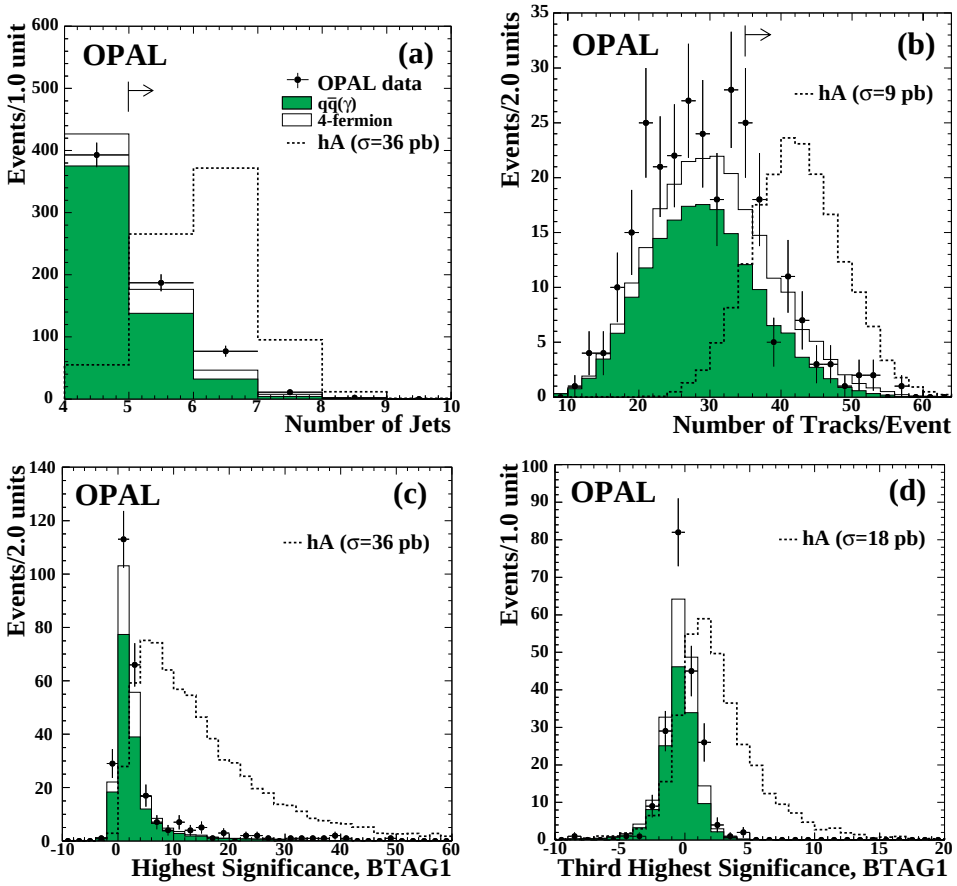

Fig. 7a–d. Selection variables relevant for the $h^0A^0 \to b\bar{b}b\bar{b}b\bar{b}$ analysis. **a** The number of reconstructed jets using the Durham algorithm with $y_{\rm cut} = 0.0015$ after multihadronic event selection and application of cut (3), for events with four or more jets, **b** the charged track multiplicity after cut (3), **c** the highest secondary vertex significance for the BTAG1 algorithm (see Sect. 2 for definition) after cut (3), **d** the third-highest secondary vertex significance for the BTAG1 algorithm after cut (3). The distributions are added for the centre-of-mass energies 130–136 GeV, 161 GeV and 170–172 GeV. Data are indicated by points. The shaded histograms show the $q\bar{q}(\gamma)$ background, and the open histograms show the four-fermion background, normalised to the integrated luminosity of the data. Two-photon processes are not included. The dashed lines represent a simulated signal with $m_{\rm h} = 60\,{\rm GeV}$, $m_{\rm A} = 30\,{\rm GeV}$ for $\sqrt{s} = 171\,{\rm GeV}$, where the displayed production cross-sections have been chosen for visibility. Arrows indicate domains accepted by the selection

Table 5. Also shown are the detection efficiencies for simulated samples of $e^+e^- \to h^0A^0 \to A^0A^0A^0 \to b\bar{b}b\bar{b}b\bar{b}$ with $m_{\rm h} = 60\,{\rm GeV}$ and $m_{\rm A} = 30\,{\rm GeV}$. No events pass the selection requirements for any of the three data samples, consistent with the background expectations of 0, 0.23, 0.37 events for the 130–136, 161, 170–172 GeV samples, respectively.

The systematic errors on the detection efficiencies for the signal are dominated by the statistics of the 500-event Monte Carlo samples, typically 7%. In addition to the statistical errors, there are errors due to the modelling of the selection variables. A Monte Carlo sample of 10 000 events with $m_{\rm h} = 60\,{\rm GeV}$, $m_{\rm A} = 30\,{\rm GeV}$ for $\sqrt{s} = 171\,{\rm GeV}$ was used to study systematic effects. The most significant of these effects on the efficiencies is the b-tagging requirement, where the modelling of the b fragmentation and lifetime and the vertex finding algorithms can introduce systematic effects. These effects are similar to those for the $h^0A^0 \to b\bar{b}b\bar{b}$ analysis. The distributions of the significances of the first, second and third most significant vertices agree within the limited statistics between data and the $(Z^0/\gamma)^* \to q\bar{q}(\gamma)$ simulation for the selection variables of this analysis. The systematic errors on the efficiency due to the b-tagging requirement were found to be 1.7% due to the impact parameter resolution and fragmentation uncertainties and 3.5% due to the b-hadron decay multiplicity uncertainty. The systematic errors due to the jet reconstruction, the requirement on $\sqrt{s'}$, and the track multiplicity are 1.2%, 1.7% and 7.2%, respectively. The total systematic error on the detection efficiency, not including Monte Carlo statistics, is thus 8.5%. Additional systematic errors on the predicted total numbers of events arise from the error on the integrated luminosity (0.6%) [21] and the theoretical uncertainty on the cross-section (1%).

The systematic errors on the background estimates similarly include contributions from the modelling of the distributions used in the event selection and from Monte Carlo statistics. As mentioned previously, the PYTHIA

Table 5. Effect of the selection criteria on data, background (normalised to the integrated luminosity of the data) and signal simulation ($m_{\mathrm{h}} = 60\,\mathrm{GeV}$, $m_{\mathrm{A}} = 30\,\mathrm{GeV}$) at the three centre-of-mass energies for the signal channel $\mathrm{h^0A^0}\to\mathrm{b\bar{b}b\bar{b}b\bar{b}}$. The quoted errors on the background are statistical

$\sqrt{s} = 130$–$136\,\mathrm{GeV}$					
Cut	Data	Total Bkg.	$\mathrm{q\bar{q}}(\gamma)$	4f	$\epsilon(\%)$
(1)	1536	1489	1478	11	98
(2)	278	232	229	2.8	90
(3)	83	65.2	63.1	2.1	77
(4)	7	10.4	10.1	0.3	63
(5)	0	<0.08	0	0	22
$\sqrt{s} = 161\,\mathrm{GeV}$					
Cut	Data	Total Bkg.	$\mathrm{q\bar{q}}(\gamma)$	4f	$\epsilon(\%)$
(1)	1499	1399	1346	53.2	100
(2)	220	175	158	17.1	91
(3)	95	75.4	59.8	15.6	84
(4)	14	17.0	11.3	5.7	71
(5)	0	0.23±0.04	0.16	0.07	34
$\sqrt{s} = 170$–$172\,\mathrm{GeV}$					
Cut	Data	Total Bkg.	$\mathrm{q\bar{q}}(\gamma)$	4f	$\epsilon(\%)$
(1)	1403	1254	1137	117.3	100
(2)	223	164.5	124	40.5	90
(3)	99	91.2	52.0	39.2	83
(4)	32	27.4	10.8	16.6	70
(5)	0	0.37±0.05	0.26	0.11	32

generator underestimates the number of radiative events with five or more jets (72% of the events have $\sqrt{s'} < 150\,\mathrm{GeV}$ for the highest energy sample) by about 55% after cut (1) for the 170–172 GeV sample. Also the high-end tail of the charged track multiplicity distributions could be mismodelled. The background estimate is also subject to the modelling of higher-order QCD processes. In addition, the tagging of the third most significant vertex as a b is subject to the misidentification of jets which do not result from b quarks, as in the $\mathrm{h^0A^0}\to\mathrm{b\bar{b}b\bar{b}}$ analysis. To estimate all these sources of systematic errors related to the modelling of the Standard Model physics, the backgrounds calculated using the HERWIG Monte Carlo were compared with those from PYTHIA. The HERWIG Monte Carlo describes the jet rates of the data much better. The differences between PYTHIA and HERWIG in the predicted numbers of background events passing all selection requirements are −0.15, −0.03, 0.03 events for $\sqrt{s} = 130$–136, 161, 170–172 GeV and are consistent with zero within one standard deviation. These are less than the statistical errors on the predictions from either Monte Carlo generator, which for PYTHIA are 100%, 17%, 15% for the 130–136, 161, 170–172 GeV Monte Carlo samples, respectively. The systematic errors due to the b-tagging, jet reconstruction, $\sqrt{s'}$, and track multiplicity requirements were estimated to be 3.2%, 5.5%, 4.4%, and 13.5%, respectively, using the same methods as were used to calculate the systematic errors on the detection efficiencies. Thus the systematic error on the background is dominated by the statistical error and amounts to approximately 100%, 23%, 21% for the 130–136, 161, 170–172 GeV Monte Carlo samples, respectively. Since for this channel the predicted backgrounds are very small, no background subtraction is applied.

5 Statistical combination of individual search channels

The searches for Higgs bosons performed by OPAL have not led to any significant signals. The negative results in individual search channels, based on data at various centre-of-mass energies, are statistically combined to increase the sensitivity. A new statistical method [16], based on "fractional event counting", is used for that purpose. The method is used to test the predictions of specific models (e.g. the MSSM or Two Higgs Field Doublet Model) for specific parameter sets by comparing them to the experimental results.

The method assigns a weight to each candidate event for a given hypothetical Higgs mass m (test mass). The sum of weights for all candidates is used as a test variable X to extract the confidence limit. The probabilities $CL_{\mathrm{s+b}}$ and CL_{b} that the test variable X does not exceed the observed value under a signal-plus-background hypothesis or a background-only hypothesis are computed analytically. Because there is the possibility that the observation X is less than the average background-only prediction, an upper bound for the confidence limit is computed according to $CL = CL_{\mathrm{s+b}}/CL_{\mathrm{b}}$. In the limit of a uniform mass distribution this ansatz gives the result for a counting experiment, using Bayesian integration.

The weight, $w_{ij}(m)$, for each candidate j of each search channel i at the test mass m is determined by the product of a channel scaling factor, $c_i(m)$, and another factor, $f_i(m, m_{ij})$, which is determined by the expected mass distribution at m evaluated at the candidate mass, m_{ij}.

The channel scaling factors c_i are determined by the signal-to-background ratio:

$$c_i(m) = \left(1 + \frac{B_i(m) \cdot s(m)}{S_i^{max}(m) \cdot s_i(m)}\right)^{-1}.$$

The expected number of signal events in channel i, $s_i(m)$, is calculated using the model prediction for the cross-section and branching ratio, the integrated luminosity of the data set to which the search is applied,[5] and the signal detection efficiency. The total expected signal rate is $s(m) = \sum_i s_i(m)$. The function $S_i(m, m_{ij})$ is the signal probability density. Its maximum for any possible m_{ij} is

[5] Identical search channels using different data sets are considered as individual channels

$S_i^{\max}(m)$. The function $B_i(m)$ is the expected differential background rate per GeV for test mass m. For channels where the mass is reconstructed, $S_i^{\max}(m)$ is inversely proportional to the mass resolution. For channels without mass reconstruction, the ratio $B_i(m)/S_i^{\max}(m)$ is replaced by the total background rate. This implies that the c_i are larger for channels where the mass is reconstructed.

The factor $f_i(m, m_{ij})$ is given by the ratio

$$f_i(m, m_{ij}) = \frac{S_i(m, m_{ij})}{S_i^{\max}(m)}.$$

The overall event weight for each candidate is thus given by:

$$w_{ij}(m) = K \cdot c_i(m) \cdot f_i(m, m_{ij}).$$

The factor K is a normalisation constant that fixes the largest value of $w_{ij}(m)$ to unity.

The sum of candidate weights over all channels $w(m) = \sum_{i,j} w_{ij}(m)$ is converted to a confidence level $CL(m)$ [16] for this sum to be more likely due to signal-plus-background than due to background-only. For example for $CL = 0.05$, the signal hypothesis is rejected at 95% confidence level.

In some channels as indicated previously, the background is statistically subtracted from the data to enhance the search sensitivity. In these cases, the subtracted background is first conservatively reduced by its systematic error. In calculating the c_i the best estimate of the background is always taken.

The uncertainty on the signal detection efficiency is accounted for using the method described in [44].

There is an overlap between some search channels in selected signal and background events. In the case of overlap in the signal, there is the problem of assigning the correct weight to a candidate. This situation did not not occur for the search results of this paper, because the efficiency of a given search channel for the topology of any other channel is taken to be zero. Overlap in the background is only relevant when the background is subtracted from the data in areas where the same candidate is found simultaneously in different search channels. This situation does not occur for the candidate events found in the search channels used here.

6 Model-independent and Two Doublet Model interpretations

Model-independent limits are given for the cross-section for the generic processes $e^+e^- \to S^0Z^0$ and $e^+e^- \to S^0P^0$, where S^0 and P^0 denote scalar and pseudo-scalar neutral bosons, respectively. The limits are conveniently expressed in terms of scale factors, s^2 and c^2, which relate the cross-sections of these generic processes to those of well-known SM cross-sections (c.f. (1), (2)):

$$\sigma_{SZ} = s^2 \, \sigma_{HZ}^{SM}, \quad (3)$$

$$\sigma_{SP} = c^2 \, \bar{\lambda} \, \sigma_{\nu\bar{\nu}}^{SM}. \quad (4)$$

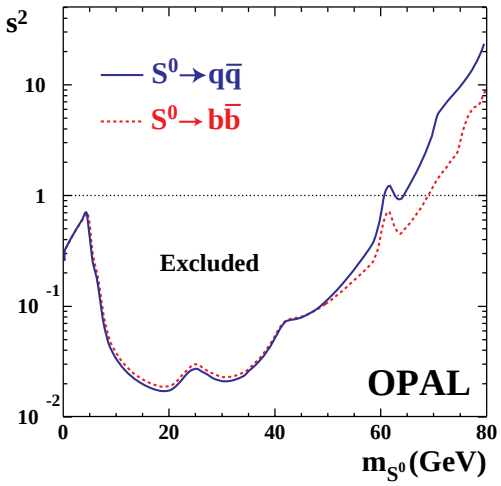

Fig. 8. Upper limits at 95% CL on s^2 (as defined by (3)) using all SM search channels and assuming the SM Higgs branching ratios for the S^0 (dashed line), and discarding all search channels that use b-tagging but assuming a hadronic branching ratio of the S^0 of 100% (solid line)

Figure 8 shows the 95% CL upper bound for s^2 as a function of the S^0 mass, obtained from:

$$s^2 = \frac{N_{95}^{SZ}}{\sum (\epsilon \, \mathcal{L} \, \sigma_{HZ}^{SM})},$$

where N_{95}^{SZ} is the 95% CL upper limit for the number of possible signal events in the data, ϵ is the signal detection efficiency and $\mathcal{L}$ is the integrated luminosity. The sum runs over the different centre-of-mass energies considered. The dashed line is computed using all search channels and assumes SM Higgs branching ratios for the S^0. The solid line is computed assuming 100% hadronic branching ratio for the S^0 and uses only search channels that do not employ b-tagging and is therefore more generally valid. Below $m_{S^0} \approx 5\,\text{GeV}$, the direct search loses sensitivity rapidly and the limit for s^2 is determined from Γ_{Z^0} only, as described below.

Figure 9 shows contours of 95% CL upper limits for c^2 in the S^0 and P^0 mass plane, for the processes $e^+e^- \to S^0P^0 \to b\bar{b}b\bar{b}$ and $q\bar{q}\tau^+\tau^-$, respectively. In both cases a 100% branching ratio into the specific final state is assumed. The contours are obtained from:

$$c^2 = \frac{N_{95}^{SP}}{\sum (\epsilon \, \mathcal{L} \, \bar{\lambda} \, \sigma_{\nu\bar{\nu}}^{SM})},$$

with N_{95}^{SP} being the 95% CL upper limit for the number of signal events in the data. The results obtained for $b\bar{b}b\bar{b}$ (Fig. 9a) are symmetric with respect to interchanging S^0 and P^0 while those obtained for $\tau^+\tau^-q\bar{q}$ are not. For this reason, the results for $\tau^+\tau^-q\bar{q}$ (Fig. 9b) are presented with the mass of the particle decaying into $\tau^+\tau^-$ along the abscissa and that of the particle decaying into $q\bar{q}$ along the ordinate. The irregularities of the iso-c^2 contours are due to the presence of candidate events that affect N_{95}^{SP}.

If the decay of the Z^0 into a final state containing S^0 or P^0 is possible, the width Γ_Z will be larger than when only

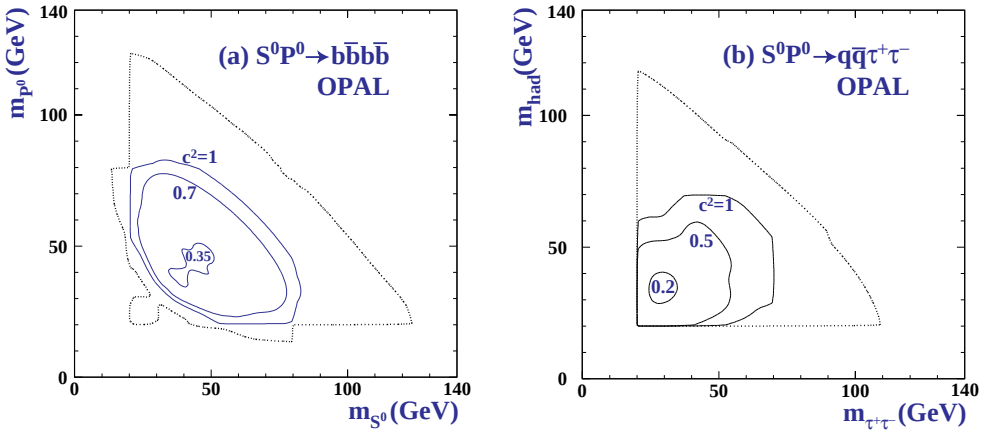

Fig. 9a,b. Upper limits at 95% CL for c^2 (see (4)) for: **a** the $S^0P^0 \to b\bar{b}b\bar{b}$ search channel assuming the $b\bar{b}$ branching ratio for both S^0 and P^0 to be 100%, **b** the $S^0P^0 \to q\bar{q}\tau^+\tau^-$ search channel assuming a 100% branching ratio for this final state. The invariant masses of the tau-lepton pair and hadron jet-pair are denoted $m_{\tau\tau}$ and m_{had}, respectively. The search efficiency is zero outside this area surrounded by the dotted line

the known Standard Model decays are possible. The excess width that is still possible when subtracting the predicted Standard Model width from the measured Γ_{Z} value can be used to place upper limits on the cross-sections of Z^0 decays into final states with S^0 or P^0 bosons. The additional width of the Z^0 resonance from final states not classified as lepton pairs can be extracted from the measurement of the branching ratio $\mathrm{BR}(\mathrm{Z}^0 \to \ell\ell) = \Gamma(\mathrm{Z}^0 \to \ell\ell)/\Gamma(\mathrm{Z}^0 \to \mathrm{all})$. The limits obtained from this equation are not sensitive to radiative corrections that equally affect all final states, because these cancel in the ratio. The current measurement is $\mathrm{BR}(\mathrm{Z}^0 \to \ell\ell) = 0.03366 \pm 0.00006$ [45]. From this value and the predicted SM value obtained from [46], the difference between the measured and predicted Z^0 width is $(-1.2 \pm 4.4(\mathrm{exp}) \pm 1.7(\mathrm{QCD}) \pm 1.8\ (\mathrm{EW}))$ MeV, resulting in an excess width less than 7.1 MeV at 95% CL. The uncertainties are due to experimental errors, QCD corrections and electroweak corrections, respectively. This excess width of the Z^0 can still be affected by corrections, such as vertex corrections and oblique corrections, that are different for different final states. However, these corrections are expected to be small for the Two Higgs Field Doublet Model (2HDM). In the case of a very light Higgs ($m_{\mathrm{h}} < 2m_{\mu}$) that remains invisible or that decays into photons, electrons, or muons, some of the final states $\mathrm{Z}^*\mathrm{S}^0$ with the Z^* decaying to leptons could still be classified as a lepton pair and the above limit does not apply. However, in this case the decay-mode-independent search limit of [47] is applied.

In the 2HDM the bosons S^0 and P^0 are identified with h^0 and A^0, and the couplings s^2 and c^2 are identified with $\sin^2(\beta-\alpha)$ and $\cos^2(\beta-\alpha)$, respectively. The assignment of the possible excess width in Γ_{Z} to the process $\mathrm{Z}^0 \to \mathrm{h}^0\mathrm{Z}^*$ yields an upper bound for s^2 which depends only on the mass of h^0; the assignment to $\mathrm{Z}^0 \to \mathrm{h}^0\mathrm{A}^0$ yields an upper bound for c^2 which depends on the masses of both h^0 and A^0. Combining these limits, the black region in the mass plane shown in Fig. 10 is excluded at 95% CL regardless of h^0 and A^0 decay modes. In the 2HDM, disregarding the possibility of $\mathrm{h}^0 \to \mathrm{A}^0\mathrm{A}^0$, the most important final states of the decays of the h^0 and A^0 bosons are $b\bar{b}$, $c\bar{c}$ and $\tau^+\tau^-$. The branching ratios depend on $\tan\beta$, but the hadronic branching fraction always exceeds 92% [48]. For $\tan\beta \geq 1$ the $b\bar{b}$ channel dominates while for $\tan\beta < 1$ the $c\bar{c}$ contribution may become the largest.

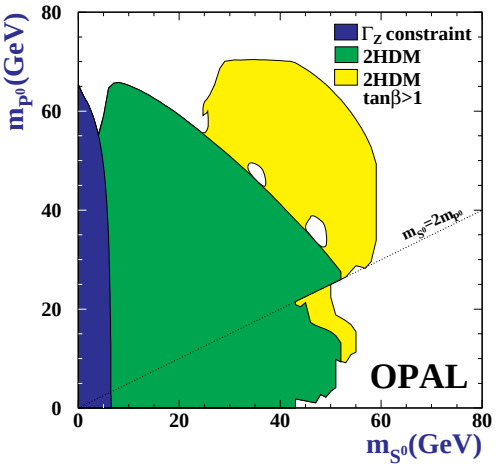

Fig. 10. Regions excluded at 95% CL in the Type II 2HDM. The black region is excluded using constraints from Γ_{Z} only. The dark grey region uses the direct searches for the SM Higgs in addition, but discarding the search channels that use b-tagging, assuming a hadronic branching ratio of the h^0 of 92%. The light grey region is excluded for $\tan\beta > 1$ in the 2HDM, assuming SM Higgs branching ratios for h^0 and A^0

In Fig. 10 the excluded area in the $(m_{\mathrm{h}}, m_{\mathrm{A}})$ plane is shown when the limits on c^2 and s^2 are combined. Below the dotted line, where the $\mathrm{h}^0 \to \mathrm{A}^0\mathrm{A}^0$ decay is kinematically allowed and competes with the $\mathrm{h}^0 \to \mathrm{f}\bar{\mathrm{f}}$ decay, the smaller of the detection efficiencies is used. The excluded area is therefore valid regardless of the $\mathrm{h}^0 \to \mathrm{A}^0\mathrm{A}^0$ branching ratio. The dark grey area is excluded at 95% CL when $\mathrm{BR}(\mathrm{h}^0 \to \mathrm{q}\bar{\mathrm{q}}) \geq 92\%$, generally valid in the 2HDM. The limit in the 2HDM for equal h^0 and A^0 masses is at $m_{\mathrm{h}} = m_{\mathrm{A}} = 41.0\,\mathrm{GeV}$.[6] The light grey area is excluded when SM Higgs branching ratios are assumed for h^0 and A^0. This assumption is valid in the 2HDM for $\tan\beta > 1$. In that case the limit for equal h^0 and A^0 masses is at $m_{\mathrm{h}} = m_{\mathrm{A}} = 56.0\,\mathrm{GeV}$. The holes in the exclusion of

[6] Throughout this paper numerical mass limits are quoted to 0.5 GeV precision

the light grey area at the edge of the dark grey excluded region are caused by the single candidate event in the $h^0A^0 \to b\bar{b}b\bar{b}$ search.

7 Interpretations of the search results in the MSSM

In its most general form, the MSSM has more than one hundred parameters. In this paper we consider a constrained MSSM, with only five free parameters in addition to those of the SM. The model assumes unification of the scalar-fermion masses (m_0) at the grand unification (GUT) scale, and unification of the gaugino masses (which are parametrised using M_2, the SU(2) gaugino mass term at the electroweak scale) and scalar-fermion tri-linear couplings (A) at the electroweak scale. These simplifications have practically no impact on the MSSM Higgs phenomenology. In particular, a common scalar-fermion mass and tri-linear coupling is justified since only the scalar top ($\tilde{t}$) sector gives important contributions to Higgs boson masses and couplings.

Other free parameters of the model are the supersymmetric Higgs mass parameter μ, $\tan\beta$, and the mass of the CP-odd neutral Higgs boson, m_A. As mentioned previously, the top quark mass has a strong impact on m_h. Therefore, it is also varied within reasonable bounds.

In scanning the MSSM parameter space, values of the above parameters are input to the HZHA event generator [30,48] which is supplemented with parts of the SUSYGEN [49] program. The HZHA program provides the masses and couplings of all Higgs bosons as well as those of the supersymmetric partners. It also calculates the cross-sections for $e^+e^- \to h^0Z^0$ and h^0A^0 [50] at each centre-of-mass energy, corrected for initial-state radiation. SUSYGEN produces scalar-fermion masses on the electroweak scale, starting from the same input parameters.

For the above parameters, the following ranges are considered:

- m_0: 0 to 1000 GeV. The masses of physical scalar-fermions are obtained in SUSYGEN by running m_0 from the GUT scale down to the electroweak scale using the relevant renormalisation group equations.
- M_2: 0 to 2000 GeV. The U(1) and SU(3) gaugino mass terms, M_1 and M_3, are calculated from M_2 using the ratios of the corresponding coupling constants, $M_1 : M_2 : M_3 = \alpha_1 : \alpha_2 : \alpha_3$.
- A: $-2.5 \cdot m_0$ to $2.5 \cdot m_0$. This range is chosen to include all possible $\tilde{t}$ mixings.
- μ: -1000 to 1000 GeV.
- m_A: 5 to 160 GeV. Beyond this range, values in 5 GeV slices around m_A = 250, 400, 1000 and 2000 GeV are also explored. Masses below 5 GeV are not considered since in that domain the decays of A^0 are uncertain. As discussed in the previous section and shown in Fig. 10, for $m_h < 43.0$ GeV, small values of m_A are excluded on more general grounds. Note that the parameter m_A which is used as input to HZHA and SUSYGEN is the "running mass", while the mass of the CP-odd Higgs boson A^0, which is used to express the results, is the physical mass.
- $\tan\beta$: 0.7 to 50. This spans the theoretically favoured range, $1 < \tan\beta < m_t/m_b$, but also includes values less than unity, which are not ruled out by theory.
- m_t: 165, 175 and 185 GeV. The range of values includes approximately two standard deviations of the measured top quark mass [12].

Most parameters are scanned by dividing their ranges into bins of variable size and choosing the values in each bin at random ("stratified scanning"). Exceptions are the parameter m_t, for which three discrete values are used, and the values of m_A greater than 160 GeV, for which 5 GeV bands around the values are used.

The following parameter scans are considered in order of increasing complexity:

(A) The parameters m_0 and M_2 are fixed at 1 TeV, μ is fixed at -100 GeV and $m_t = 175$ GeV. The parameter A is fixed to 0 (minimal $\tilde{t}$ mixing) or $\sqrt{6} m_Q$ (maximal $\tilde{t}$ mixing.) The mass m_Q of the "left-up" scalar quark at the electroweak scale is uniquely determined in terms of m_0 and the other input parameters [49]. The parameters m_A and $\tan\beta$ are varied as described above. This simple scan serves as a *benchmark* corresponding to the scans proposed in [10].

(B) We also consider two scans which correspond to cases of *minimal and maximal mixing* in the $\tilde{t}$ sector, inducing small and large corrections to the h^0 boson mass, respectively. In these scans the parameters m_0, M_2, m_A, $\tan\beta$, and m_t are varied independently, μ is constrained to $-0.1 m_Q$ and the parameter A is set to
  - $A = 0$ for minimal mixing, and
  - $A = \sqrt{6}\ m_Q$ for maximal mixing.

(C) In the most *general scan* considered here, all parameters described previously are varied independently in the ranges that are listed above.

The number of parameter sets considered in scan (A) is about 50 000, that of the scan (B) is approximately 1 000 000, and that of scan (C) is close to 6 000 000.

Before comparing the above parameter sets to the data, these are subject to a selection on the basis of theoretical and experimental considerations. Only those sets are selected that provide a $\tilde{t}_1$ mass larger than the lightest neutralino mass. Additional experimental constraints are applied, which do not relate directly to the searches described here. A parameter set is rejected if the sum of the partial decay widths of $Z^0 \to h^0Z^*$ and $Z^0 \to h^0A^0$ is more than 7.1 MeV (see the discussion of the constraint from Γ_Z in Sect. 6). Parameter sets giving rise to chargino or neutralino masses [23], or stop masses [51] excluded by OPAL searches at LEP2 are also discarded.

It has been shown [52] that large values of A and μ may give rise to non-zero vacuum expectation values for the $\tilde{t}$ fields which break charge and colour symmetry. Criteria for charge- and colour-breaking (CCB) minima of the MSSM Lagrangian have been determined [53], but these may be substantially modified if also "tunneling" from the electroweak minimum to a lower lying CCB minimum is

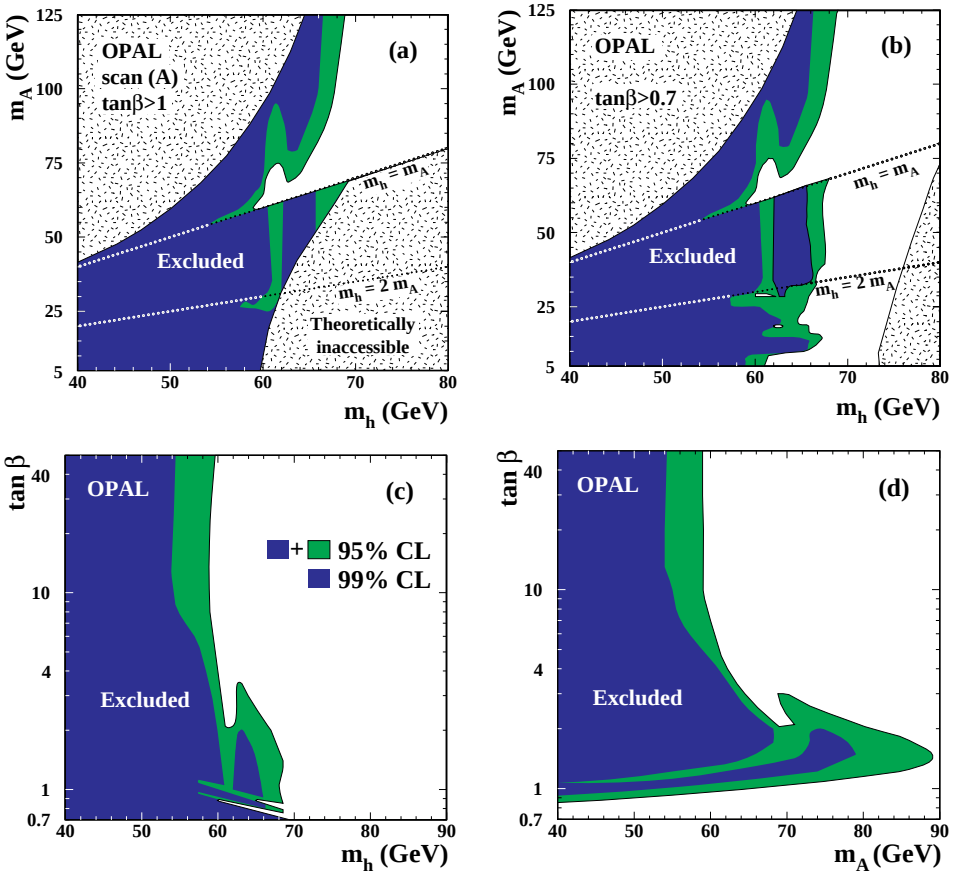

Fig. 11a–d. The MSSM exclusion for scan (A) described in the text of Sect. 7. Excluded regions are shown for **a** the (m_{h}, m_{A}) plane for $\tan\beta > 1$, **b** the (m_{h}, m_{A}) plane for $\tan\beta > 0.7$, **c** the (m_{h}, $\tan\beta$) plane, and **d** the (m_{A}, $\tan\beta$) plane. The black areas are excluded at 99% CL. The black plus the dark grey areas are excluded at 95% CL. The speckled areas in **a** and **b** are theoretically inaccessible

taken into account. A calculation that includes the effect of tunneling is available for one specific scenario out of a number of distinct possibilities [54], but a complete treatment of CCB criteria is not yet available to our knowledge. A simple approximate criterion to avoid CCB minima is [52]:

$$A^2 + 3\mu^2 < x(m_{\tilde{\mathrm{t}}_{\mathrm{L}}}{}^2 + m_{\tilde{\mathrm{t}}_{\mathrm{R}}}{}^2)\,, \qquad (5)$$

where $m_{\tilde{\mathrm{t}}_{\mathrm{L}}}$ and $m_{\tilde{\mathrm{t}}_{\mathrm{R}}}$ denote the left- and right-handed scalar top masses and $x{\approx}3$. For the specific calculation that includes tunneling this bound was shown to be modified to $x{\approx}7.5$ [54]. For the general scan (C) of the MSSM parameter space results will be shown without applying CCB criteria, and for CCB criteria applied with $x = 3$ and $x = 7.5$.

The experimental exclusion limits, at the 95% CL, are presented below, separately for the scans (A), (B), and (C). In each scan the total predicted number of events from all search channels is calculated using cross-sections, branching ratios, luminosities and search efficiencies for all different MSSM parameter sets. From this expected signal prediction and the number of observed events a confidence level is calculated according to the prescription in Sect. 5. For scans (A) and (B) the 99% CL exclusion is also shown, to indicate the sensitivity to the chosen exclusion confidence level. The results are presented for each scan in four figures: (a) in the (m_{h}, m_{A}) plane for $\tan\beta > 1$, (b) in the same plane for $\tan\beta > 0.7$, (c) in the (m_{h}, $\tan\beta$) plane, and (d) in the (m_{A}, $\tan\beta$) plane. For scans (A) and (B) the lower limits for the minimal and maximal mixing cases differ by only small amounts and only the weaker of the two exclusion limits is given. The theoretically accessible area corresponds to the larger one, for maximal stop mixing. The theoretically inaccessible areas are shown in the figures as speckled.

The results for scan (A) are shown in Fig. 11. The structure near $m_{\mathrm{h}} = 60\,\mathrm{GeV}$ is caused by the candidate in the analysis for the LEP1 leptonic channel at $m_{\mathrm{h}} = 61.2\,\mathrm{GeV}$. From Fig. 11a, for $\tan\beta > 1$, 95% CL lower limits can be obtained for $m_{\mathrm{h}} > 59.0\,\mathrm{GeV}$ and $m_{\mathrm{A}} > 59.5\,\mathrm{GeV}$. When the $\tan\beta$ range is enlarged to $\tan\beta > 0.7$ (Fig. 11b), the lower limit of m_{h} is not affected, but no lower limit on m_{A} can be given. Figures 11a and b show the region $m_{\mathrm{A}} > 5\,\mathrm{GeV}$. For $m_{\mathrm{A}} < 5\,\mathrm{GeV}$ and $m_{\mathrm{h}} > 43\,\mathrm{GeV}$ the value of $\sin^2(\beta-\alpha)$ is always very close to unity in scan (A). Therefore, in this region only the $\mathrm{Z}^0\mathrm{h}^0$ production process is relevant for the exclusion, and the limit depends neither on m_{A} nor on the A^0 decay modes. Hence, the limit for m_{h} at $m_{\mathrm{A}} = 5\,\mathrm{GeV}$ is also valid for $m_{\mathrm{A}} < 5\,\mathrm{GeV}$. Figure 11c shows the projection onto the (m_{h}, $\tan\beta$) plane. Large values of $\tan\beta$ correspond to $m_{\mathrm{h}}{\approx}m_{\mathrm{A}}$. In the ($m_{\mathrm{A}}$, $\tan\beta$) projection of Fig. 11d the strongest limit for m_{A} of 89.0 GeV at 95% CL is obtained at $\tan\beta{\approx}1.4$. However, at 99% CL this limit drops considerably.

Figure 12 shows the results for scan (B). Differences with respect to scan (A) are due to the possibility of hav-

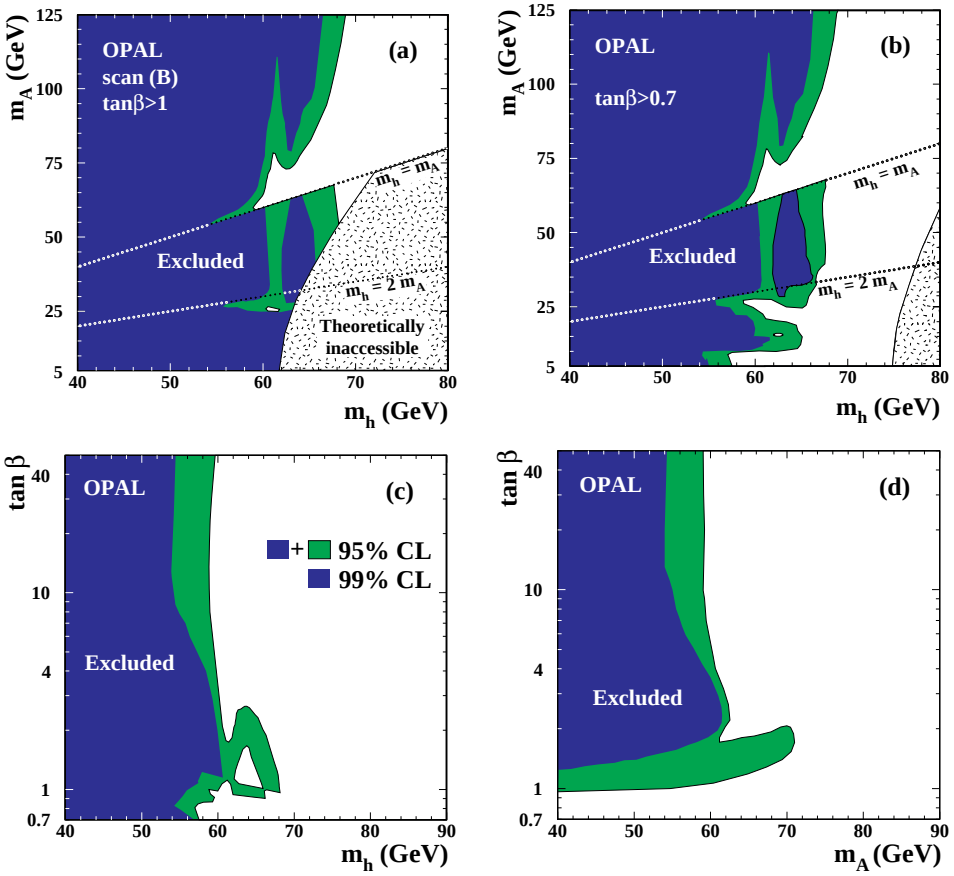

Fig. 12a–d. The MSSM exclusion for the scan (B) described in the text of Sect. 7. Excluded regions are shown for **a** the (m_h, m_A) plane for $\tan\beta > 1$, **b** the (m_h, m_A) plane for $\tan\beta > 0.7$, **c** the (m_h, $\tan\beta$) plane, and **d** the (m_A, $\tan\beta$) plane. The black areas are excluded at 99% CL. The black plus the dark grey areas are excluded at 95% CL. The speckled areas in **a** and **b** are theoretically inaccessible

ing lower $m_{\tilde{\mathrm{t}}}$ values. This leads in general to modified couplings and in particular, for some parameter sets, to a strongly enhanced branching ratio for $\mathrm{h}^0 \to \mathrm{gg}$. The wider range of $m_{\tilde{\mathrm{t}}}$ in conjunction with $m_\mathrm{t} = 185\,\mathrm{GeV}$ leads to larger theoretically accessible regions. Despite these modifications, many essential features such as the limit for m_h at very high m_A, the limits for m_h and m_A near $m_\mathrm{h} = m_\mathrm{A}$ and the absolute lower limit on m_h remain unchanged. The absolute lower limit on m_A for scan (B) is $m_\mathrm{A} > 23.0\,\mathrm{GeV}$ at 95% CL, but the range $26.5 < m_\mathrm{A} < 55.0\,\mathrm{GeV}$ is excluded at 95% CL. The small unexcluded "island" at $60.5 < m_\mathrm{h} < 61.5\,\mathrm{GeV}$ and $23.0 < m_\mathrm{A} < 26.5\,\mathrm{GeV}$ is due to the simultaneous effect of a large branching ratio for $\mathrm{h}^0 \to \mathrm{A}^0\mathrm{A}^0$ and the LEP1 leptonic channel candidate. Because the theoretically allowed region at low m_A and high m_h is increased in scan (B) with respect to that in scan (A), there is an additional unexcluded triangular region near $m_\mathrm{h} = 68\,\mathrm{GeV}$ with a minimum value at $m_\mathrm{A} = 55.0\,\mathrm{GeV}$ at 95% CL.

For the results of scan (C), shown in Fig. 13, all exclusions are at 95% CL. For this scan the exclusion regions are shown for three cases: Without the application of any CCB criterion in black, for the CCB criterion of 5 with $x = 7.5$ in black and dark grey, and with $x = 3$ in black, dark grey and light grey. The situation changes dramatically with respect to scans (A) and (B) due to the appearance of unexcluded parameter sets with small values of m_h. These points are characterised by a large mass difference $m_\mathrm{A} - m_\mathrm{h}$ and small $\sin^2(\beta-\alpha)$, hence the $\mathrm{h}^0\mathrm{Z}^0$ production is suppressed (cf. (1)). The $\mathrm{h}^0\mathrm{A}^0$ production is kinematically allowed at LEP2 energies in most of the affected region, but the cross-section is small, and the current integrated luminosity is not sufficient to exclude these parameter sets. The existence of such parameter sets has already been pointed out in [55].

If no CCB criterion is applied (the black area only is excluded), no absolute lower limit for m_h can be given (Fig. 13a and b). For the CCB criterion applied with $x = 7.5$, the unexcluded area near $m_\mathrm{h} = 5\,\mathrm{GeV}$ is due to the relatively weak limit on $\sin^2(\beta-\alpha)$ for this mass range, as shown in Fig. 8. For $x = 3$, the lower limit on m_h is 50.0 GeV at 95% CL for $m_\mathrm{A} > 5\,\mathrm{GeV}$ in Fig. 13a, and it can be seen in Fig. 13c that this limit corresponds to $\tan\beta = 50$. Such high values of $\tan\beta$ always result in $m_\mathrm{h} \approx m_\mathrm{A}$ when the soft SUSY-breaking masses are high ($> 1\,\mathrm{TeV}$.) However, as can be seen from the figures, in a general scan large values of $\tan\beta$ are not excluded for large mass differences $|m_\mathrm{A} - m_\mathrm{h}|$, due to large higher-order corrections involving a low-mass stop. For $m_\mathrm{A} < 5\,\mathrm{GeV}$ the model-independent limit applies (cf. Fig. 10). This leads, for the $x = 3$ CCB criterion, to $m_\mathrm{h} > 43.0\,\mathrm{GeV}$ at 95% CL. Figure 13c shows that there is no exclusion at all at 95% CL in the (m_h, $\tan\beta$) plane for the general scan if no CCB criterion is applied. This is due to the fact that for any (m_h, $\tan\beta$) combination the other parameters can be chosen to simultaneously generate a large m_A and a small

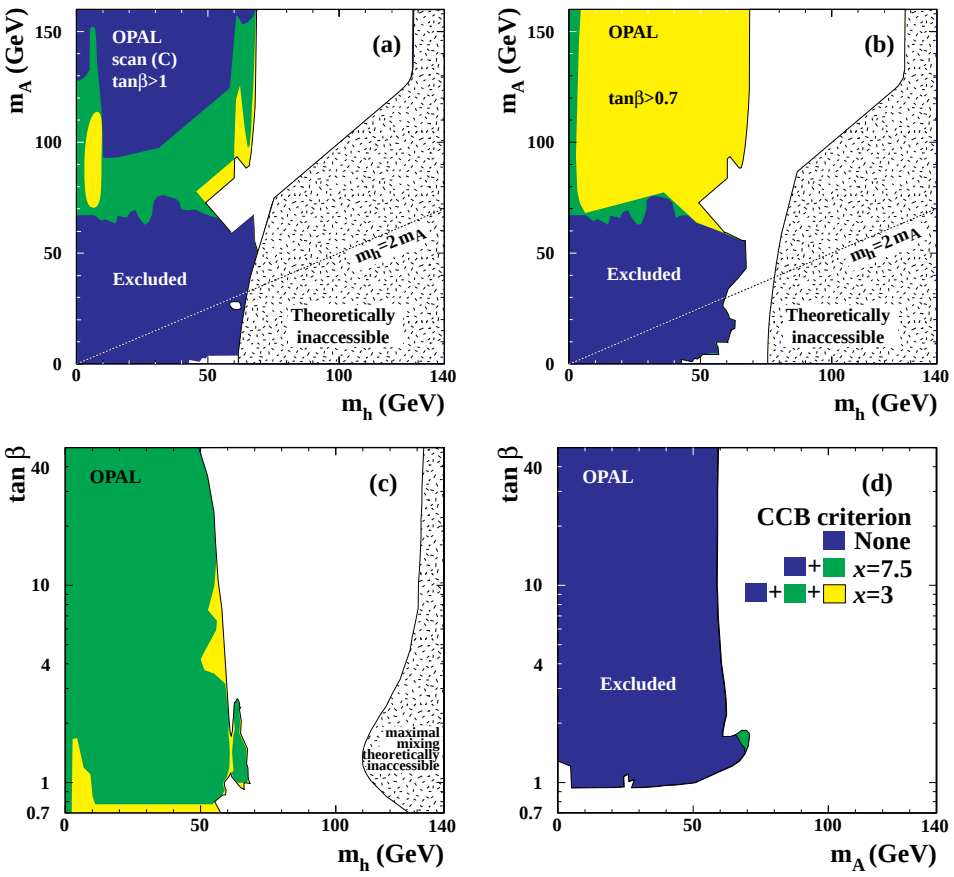

Fig. 13a–d. The MSSM exclusion for scan (C) described in the text of Sect. 7. Excluded regions are shown for **a** the $(m_{\mathrm{h}},\ m_{\mathrm{A}})$ plane for $\tan\beta > 1$, **b** the $(m_{\mathrm{h}},\ m_{\mathrm{A}})$ plane for $\tan\beta > 0.7$, **c** the $(m_{\mathrm{h}},\ \tan\beta)$ plane, and **d** the $(m_{\mathrm{A}},\ \tan\beta)$ plane. All exclusion limits are at 95% CL. The black areas are excluded without applying any CCB criterion. When the CCB criterion of 5 is applied with $x = 7.5$ the dark grey areas are excluded in addition. For this CCB criterion with $x = 3$, the black, dark grey and light grey areas are all excluded. The speckled areas in **a**, **b** and **c** are theoretically inaccessible

$\sin^2(\beta-\alpha)$. However, many of these specific parameter sets are discarded by applying a CCB criterion. In contrast, Fig. 13d, which shows the $(m_{\mathrm{A}}, \tan\beta)$ projection, is only marginally different from Fig. 11d and 12d of scans (A) and (B). The exclusion limits on m_{A} are only slightly affected.

The results in this section suggest that the MSSM parameter bounds, and in particular the limit on m_{h}, derived from the benchmark scan (A) and minimal/maximal mixing scan (B) are not valid when a more general scan (C) of the parameter space is performed.

8 Summary

Searches for neutral Higgs bosons presented here have not revealed any significant excess beyond the background expectation from SM processes. Evidence for both the $e^+e^-\to h^0Z^0$ and $e^+e^-\to h^0A^0$ production processes has been searched for, allowing also for the decay $h^0\to A^0A^0$, when kinematically possible. Limits on these processes have been placed in a model-independent manner and within the framework of the 2HDM and the MSSM. These new limits substantially improve those previously published by OPAL.

In the model-independent approach, limits have been placed on the product of cross-section and branching ratio for h^0Z^0 production assuming SM branching ratios and fully hadronic final states, and for h^0A^0 production with $b\bar{b}b\bar{b}$ and $\tau^+\tau^-q\bar{q}$ final states.

In the 2HDM interpretation, limits have been placed in the $(m_{\mathrm{h}}, m_{\mathrm{A}})$ plane both for the case of any value of $\tan\beta$ and for that of $\tan\beta > 1$. Along the h^0-A^0 mass diagonal 95% CL lower limits are set at $m_{\mathrm{h}} = m_{\mathrm{A}} > 41.0\,\mathrm{GeV}$, independently of the value of $\tan\beta$ and at $m_{\mathrm{h}} = m_{\mathrm{A}} > 56.0\,\mathrm{GeV}$ for $\tan\beta > 1$.

In the MSSM, three different scans over the model parameters have been performed. For the simplest, the benchmark scan, in which all parameters except m_{A} and $\tan\beta$ are fixed, a lower limit at 95% CL on $m_{\mathrm{h}} > 59.0\,\mathrm{GeV}$ and $m_{\mathrm{A}} > 59.5\,\mathrm{GeV}$ is derived for $\tan\beta > 1$. For $\tan\beta > 0.7$, the limit on m_{h} remains at 59.0 GeV, but no limit for m_{A} is obtained.

For the MSSM parameter scan with minimal and maximal $\tilde{t}$ mixing, where only the μ and A parameters are constrained and all other parameters are left free, the 95% CL excluded area has slightly less extent than for the benchmark scan.

In the general scan of the MSSM parameter space, parameter sets arise that cannot be excluded at 95% CL. All of these correspond to small, but non-negligible, cross-sections for the process $e^+e^-\to h^0A^0$, and will either be observed or excluded as the integrated luminosity of the data increases. A fraction of those parameter sets can be excluded if requirements are made to avoid charge- and colour-breaking vacua.

Acknowledgements. We particularly wish to thank the SL Division for the efficient operation of the LEP accelerator at all energies and for their continuing close cooperation with our experimental group. We thank our colleagues from CEA, DAPNIA/SPP, CE-Saclay for their efforts over the years on the time-of-flight and trigger systems which we continue to use. In addition to the support staff at our own institutions we are pleased to acknowledge the Department of Energy, USA, National Science Foundation, USA, Particle Physics and Astronomy Research Council, UK, Natural Sciences and Engineering Research Council, Canada, Israel Science Foundation, administered by the Israel Academy of Science and Humanities, Minerva Gesellschaft, Benoziyo Center for High Energy Physics, Japanese Ministry of Education, Science and Culture (the Monbusho) and a grant under the Monbusho International Science Research Program, German Israeli Bi-national Science Foundation (GIF), Bundesministerium für Bildung, Wissenschaft, Forschung und Technologie, Germany, National Research Council of Canada, Research Corporation, USA, Hungarian Foundation for Scientific Research, OTKA T-016660, T023793 and OTKA F-023259.

References

1. S.L. Glashow, J. Iliopoulos and L. Maiani, Phys. Rev. **D2** (1970) 1285; S. Weinberg, Phys. Rev. Lett. **19** (1967) 1264; A. Salam, *Elementary Particle Theory*, ed. N. Svartholm (Almquist and Wiksells, Stockholm, 1968), 367
2. P.W. Higgs, Phys. Lett. **12** (1964) 132; F. Englert and R. Brout, Phys. Rev. Lett. **13** (1964) 321; G.S. Guralnik, C.R. Hagen, and T.W.B. Kibble, Phys. Rev. Lett. **13** (1964) 585
3. OPAL Collaboration, K. Ackerstaff et al., E. Phys. J. **C1** (1998) 425
4. Y.A. Gol'fand and E.P. Likhtman, JETP Lett. **13** (1971) 323; D.V. Volkov and V.P. Akulov, Phys. Lett. **B46** (1973) 109; J. Wess and B. Zumino, Nucl. Phys. **B70** (1974) 39; H.E. Haber and Y. Nir, Nucl. Phys **B335** (1990) 363
5. G. 't Hooft, in *Recent Developments in Gauge Theories*, Proceedings of the NATO Advanced Summer Institute, Cargese, 1979, edited by G. 't Hooft et al.(Plenum, New York, 1980) p. 135-157; L. Susskind, Phys. Rep. **104** (1984) 181
6. H.P. Nilles, Phys. Rep. **110** (1984) 1; H.E. Haber and G.L. Kane, Phys. Rep. **117** (1985) 75; R. Barbieri et al., Z. Physics at LEP1, CERN 89–08 (1989) Vol. 2, 121; J.M. Frère, G.L. Kane, Nucl. Phys. **B223** (1983) 331; J. Ellis et al., Phys. Lett. **B123** (1983) 436; J. Ellis et al., Phys. Lett. **B127** (1983) 233
7. J.F. Gunion, H.E. Haber, G.L. Kane and S. Dawson, *The Higgs Hunter's Guide*, Addison-Wesley Publishing Company, Reading, MA, 1990
8. OPAL Collaboration, K. Ackerstaff et al., *Search for Charged Higgs bosons in e^+e^- collisions at $\sqrt{s}$ = 130–172 GeV*, CERN-PPE/97-168, to be published in Phys. Lett. **B**
9. A. Djouadi et al., Proceedings e^+e^- collisions at 500 GeV: The Physics Potential, Munich–Annecy–Hamburg, ed. P.M. Zerwas, DESY 92-123A
10. E. Accomando et al., *Higgs Physics* in *Physics at LEP2*, Editors: G. Altarelli, T. Sjöstrand and F. Zwirner, CERN 96–01 (1996)
11. M. Carena, J.R. Espinosa, M. Quirós and C.E.M. Wagner, Phys. Lett. **355B** (1995) 209
12. CDF Collaboration, F. Abe et al., Phys. Rev. Lett. **74** (1995) 2626; D0 Collaboration, S. Abachi et al., Phys. Rev. Lett. **74** (1995) 2632
13. OPAL Collaboration, R. Akers et al., Z. Phys. **C64** (1994) 1
14. OPAL Collaboration, G. Alexander et al., Z. Phys. **C73** (1997) 189
15. OPAL Collaboration, G. Alexander et al., Phys. Lett. **B377** (1996) 273
16. P. Bock, *Determination of exclusion limits for particle production using different decay channels with different efficiencies, mass resolutions and backgrounds*, Heidelberg Institute Preprint HD-PY96–05 (1996)
17. ALEPH Collaboration, D. Buskulic et al., Phys. Lett. **B313** (1993) 312; ALEPH Collaboration, R. Barate et al., Phys. Lett. **B412** (1997) 173; DELPHI Collaboration, P. Abreu et al., Z. Phys. **C67** (1995) 69; DELPHI Collaboration, P. Abreu et al., E. Phys. J. **C2** (1998) 1. L3 Collaboration, O. Adriani et al., Z. Phys. **C57** (1993) 355; L3 Collaboration, M. Acciarri et al., Phys. Lett. **B385** (1996) 454
18. OPAL Collaboration, K. Ahmet et al., Nucl. Inst. and Meth. **A305** (1991) 275
19. S. Anderson et al., Nucl. Inst. and Meth. **A403** (1998) 326
20. B.E. Anderson et al., IEEE Transactions on Nuclear Science **41** (1994) 845
21. OPAL Collaboration, K. Ackerstaff et al., Phys. Lett. **B391** (1997) 221. Phys. Lett. **B**
22. OPAL Collaboration, R. Akers et al., Phys. Lett. **B327** (1994) 397
23. OPAL Collaboration, K. Ackerstaff et al., E. Phys. J. **C2** (1998) 213
24. OPAL Collaboration, M.Z. Akrawy et al., Phys. Lett. **B253** (1991) 511
25. N. Brown and W.J. Stirling, Phys. Lett. **B252** (1990) 657; S. Bethke, Z. Kunszt, D. Soper and W.J. Stirling, Nucl. Phys. **B370** (1992) 310; S. Catani et al., Phys. Lett. **B269** (1991) 432; N. Brown and W.J. Stirling, Z. Phys. **C53** (1992) 629
26. OPAL Collaboration, K. Ackerstaff et al., Z. Phys. **C74** (1997) 1; OPAL Collaboration, R. Akers et al., Z. Phys. **C66** (1995) 19
27. OPAL Collaboration, R. Akers et al., Z. Phys. **C65** (1995) 17
28. OPAL Collaboration, R. Akers et al., Phys. Lett. **B327** (1994) 411
29. OPAL Collaboration, G. Alexander et al., Z. Phys. **C52** (1991) 175
30. HZHA 2.0 generator: P. Janot, in *Physics at LEP2*, Eds. G. Altarelli, T. Sjöstrand and F. Zwirner, CERN 96–01 (1996), Vol. 2, p. 309
31. PYTHIA 5.7 and JETSET 7.4 generators: T. Sjöstrand, Comp. Phys. Comm. **82** (1994) 74; T. Sjöstrand, LU TP 95–20 and CERN-TH.7112/93 (revised August 1995)
32. EXCALIBUR generator: F.A. Berends, R. Pittau, R. Kleiss, Comp. Phys. Comm. **85** (1995) 437

33. The grc4f 1.2 generator: J. Fujimoto et al., Comp. Phys. Comm. **100** (1997) 128
34. BHWIDE generator: S. Jadach, W. Płaczek, B.F.L. Ward, in *Physics at LEP2*, edited by G. Altarelli, T. Sjöstrand and F. Zwirner, CERN 96–01, Vol. 2 (1996), p. 286; UTHEP-95–1001
35. KORALZ 4.0 generator: S. Jadach, B.F.L. Ward, Z. Wąs, Comp. Phys. Comm. **79** (1994) 503
36. PHOJET 1.05 generator: E. Budinov et al., in *Physics at LEP2*, edited by G. Altarelli, T. Sjöstrand and F. Zwirner, CERN 96–01, Vol. 2 (1996) p. 216; R. Engel and J. Ranft, Phys. Rev. **D54** (1996) 4244
37. J.A.M. Vermaseren, Nucl. Phys. **B229** (1983) 347
38. J. Allison et al., Nucl. Inst. and Meth. **A317** (1992) 47
39. OPAL Collaboration, G. Alexander et al., Z. Phys. **C52** (1991) 175
40. OPAL Collaboration, G. Alexander et al., Phys. Lett. **B376** (1996) 232
41. G. Parisi, Phys. Lett. **B74** (1978) 65; J.F. Donoghue, F.E. Low and S.Y. Pi, Phys. Rev. **D20** (1979) 2759
42. OPAL Collaboration, R. Akers, Z. Phys. **C61** (1994) 209; DELPHI Collaboration, P. Abreau, Phys. Lett. **B347** (1995) 447
43. G. Marchesini et al., Comp. Phys. Comm. **67** (1992) 465
44. R.D. Cousins, V.L. Highland, Nucl. Inst. and Meth. **A320** (1992) 331
45. R.M. Barnett et al., Phys. Rev. **D54** (1996) 1, and 1997 off-year partial update for the 1998 edition available on the PDG WWW pages (URL: http://pdg.lbl.gov/)
46. D. Bardin et al., CERN-TH 6443/92 (May 1992); Phys. Lett. **B255** (1991) 290; Nucl. Phys. **B351** (1991) 1; Z. Phys. **C44** (1989) 493; We use ${}_{ZF}I^{T}T_{E_R}$ version 5.0 with default parameters, and with the following input parameters: $m_{\mathrm{Z}} = 91.187\,\mathrm{GeV}$, $m_{\mathrm{t}} = (175\pm5)\,\mathrm{GeV}$, $\alpha(m_{\mathrm{Z}}) = 1/128.896$, $\alpha_{\mathrm{s}}(m_{\mathrm{Z}}) = 0.118\ \pm0.003$(experimental error) ±0.003(higher order correction). The prediction for the leptonic branching ratio of the Z^0 was found not to change significantly when the Higgs mass was varied between $0 < m_{\mathrm{h}} < 50\,\mathrm{GeV}$
47. OPAL Collaboration, P.D. Acton et al., Phys. Lett. **B268** (1991) 122
48. A. Djouadi, J. Kalinowski and M. Spira, *HDECAY: a Program for Higgs Boson Decays in the Standard Model and its Supersymmetric Extension*, Preprint DESY-97-079, April 1997
49. E. Accomando et al., *Event Generators for Discovery Physics*, hep-ph/9602203, Feb. 1996, and in "Physics at LEP2", eds. G. Altarelli, T. Sjöstrand and F. Zwirner, CERN 96–01, Vol. 2 (1996) 299
50. F.A. Berends and R. Kleiss, Nucl. Phys. **178** (1981) 141
51. OPAL Collaboration, K. Ackerstaff et al., Z. Phys. **C75** (1997) 409
52. J.M. Frère, D.R.T. Jones and S. Raby, Nucl. Phys. **B222** (1983) 11; L. Alvarez-Gaumé, J. Polchinski and M. Wise, Nucl. Phys. **B221** (1983) 495; J.P. Derendinger and C.A. Savoy, Nucl. Phys. **B237** (1984) 307; C. Kounnas, A.B. Lahanas, D.V. Nanopoulos and M. Quirós, Nucl. Phys. **B236** (1986) 438
53. J.A. Casas, A. Lleyda and C. Muñoz, Nucl. Phys. **B471** (1996) 3
54. A. Kusenko, P. Langacker and G. Segre, Phys. Rev. **D54** (1996) 5824
55. R. Hempfling, Phys. Lett. **B296** (1992) 121; J. Rosiek and A. Sopczak, Phys. Lett. **B341** (1995) 419